ACS OMEGA

Open Access

http://pubs.acs.org/journal/acsodf

Article

Effect of Polyvinylpyrrolidone on the Structure Development, Electrical, Thermal, and Wetting Properties of Polyvinylidene Fluoride-Expanded Graphite Nanocomposites

Reshma Haridass, Aleena Sabu, Nikhitha Augustin, Pratheep Kumar Annamalai, and Ramanujam Brahmadesam Thoopul Srinivasa Raghava*

Cite This: *ACS Omega* 2024, 9, 178−195

Read Online

ACCESS | Metrics & More | Article Recommendations | Supporting Information

ABSTRACT: Polyvinylidene fluoride (PVDF)-expanded graphite (ExGr) nanocomposites have been prepared by solution blending and melt processing methods. In the presence of polyvinylpyrrolidone (PVP), enhanced dispersion of graphite nanosheets (GNSs) in the PVDF matrix, as suggested by field emission scanning electron microscopy analysis, results in very low electrical percolation threshold (0.3 wt % ExGr). X-ray diffraction, Fourier transform infrared spectroscopy, and differential scanning calorimetry (DSC) analyses confirm the coexistence of electroactive gamma and nonpolar alpha phases. Wrapping of PVP chains around GNSs reduces the crystallinity in PVDF-ExGr nanocomposites in comparison to that in neat PVDF films, as evidenced by DSC analysis. Thermogravimetric analysis confirms enhanced thermal stability of PVDF-ExGr nanocomposites above 500 °C mainly attributed to the PVP-assisted dispersion of GNSs. The water contact angle of solution-blended PVDF-ExGr nanocomposite films increases with and without PVP in comparison to that of the neat PVDF film. Compression-molded PVDF-ExGr nanocomposites also exhibit electroactive gamma and nonpolar alpha phases of PVDF with reduction in electrical conductivity compared to solvent-cast films.

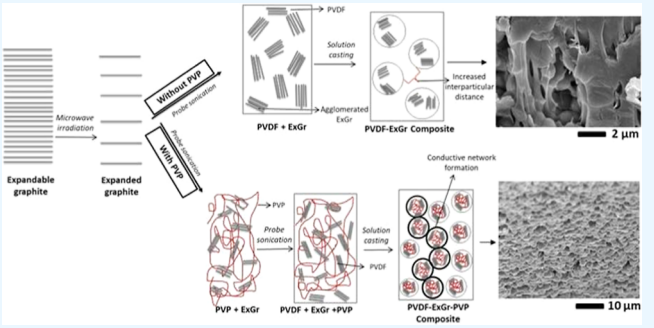

1. INTRODUCTION

Conducting polymer composites (CPCs) are being immensely focused for various applications such as sensors, actuators, fuel cell bipolar plates, energy harvesting nanogenerators, electromagnetic interference (EMI) shielding devices, etc.[1] The piezoelectric response of polymeric materials depends on electroactive phases or enhanced dipole moment changes upon mechanical deformation.[2] The EMI shielding efficiency (SE), which is a sum of shielding effect due to absorption, reflection, and multiple reflection mechanisms, depends on the electrical conductivity of the polymeric materials apart from frequency and permeability.[3] To obtain high EMI SE, the conductivity of the polymer composites should be tailor-made. The electrical conductivity of polymer composites and electroactive phases in the composites can be modulated to the desired level by the incorporation of conducting metal particles and carbonaceous fillers.[4,5] The incorporation of magnetic nanostructures along with conducting fillers in polymer matrices also improves EMI SE by the absorption mechanism.[3] The electrical percolation threshold, which is the loading of the conducting filler at which the conductivity of the composite is increased to many orders, is dependent on various parameters such as filler's particle size, aspect ratio, processing route, dispersion of fillers, and the polymer matrix.[6] It is desirable to decrease the electrical percolation threshold as *minimum* as possible, which will help in the easy processing of polymer composites. Not only retaining electrical conductivity is important, but also the mechanical properties of the composites should be improved.[7,8] In this regard, conducting carbonaceous nanofillers such as graphite nanosheets (GNSs),[9] graphene,[10] carbon nanotubes (CNTs),[11] carbon nanofibers,[12] etc., are employed for making conducting polymer nanocomposites as well as hybrid nanocomposites.

Depending on the processing route adopted for the synthesis of CPCs, the dispersion of fillers in the polymer matrix will vary. Various methods are utilized to improve the dispersion of the filler particles in a chosen polymer matrix by improving the compatibility between the fillers and the polymer matrix. In this regard, functionalizing the fillers,[13] employing surface active agents[14] and compatibilizers,[15] are more frequently

Received: May 4, 2023
Revised: November 8, 2023
Accepted: November 15, 2023
Published: December 19, 2023

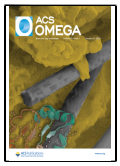

carried out. Surfactant−assisted dispersion of conducting carbonaceous nanofillers in the chosen polymer matrix is preferred rather than their functionalization. The reason is attributed to the fact that defect formation in the structure of fillers in the later process shall decrease the electrical conductivity of the composites to an appreciable level than what it would have been in the absence of functionalization of the filler particles.[16] Excess amount of surfactant can also cause the electrical conductivity of the composites to be decreased. However, the structures of the fillers would be preserved in this case. Therefore, depending on the polymer matrix, the choice and amount of surfactant used are critical for enhancing the dispersion of the filler in the polymer matrix.

Among various polymers, poly(vinylidene fluoride) (PVDF) has been chosen for this study due to its piezoelectric, ferroelectric, and pyroelectric properties. It exists in five different phases such as alpha, beta, gamma, delta, and epsilon.[17] The most stable alpha phase is nonpolar (TGTG′ configuration). Both beta (β) (TTTT configuration) and gamma (γ) phases (TTTGTTTG′ configuration) are electroactive as these phases exhibit an electric dipole moment because of the arrangement of fluorine atoms. The net dipole moment per unit cell for the beta phase is maximum (8×10^{-30} C·m).[18] Inducing the electroactive beta or gamma phase of PVDF is very important for energy harvesting applications. Though the beta phase is more polar than the gamma phase, the latter phase also exhibits a superior piezoelectric coefficient.[19] The electroactive beta phase is induced in PVDF by high-voltage poling[20] or a mechanically stretching PVDF film at elevated temperatures.[21] Other techniques such as the incorporation of fillers like graphene,[22] nano clay,[23] multi-walledCNTs,[24] etc., can result in the generation and stabilization of electroactive phases. Further, the literature suggests that various processing routes like electrospinning[25] and low-temperature crystallization of PVDF pertained to specific solvents[26] can also yield β and γ phases.

Expandable graphite is obtained after intercalating suitable acid molecules in the interplanar distance of natural graphite. Expanded graphite is obtained from the expandable graphite either by high-temperature heat treatment[27] or by microwave irradiation.[28] Usually, graphite particles are treated with potassium permanganate followed by sulfuric acid/nitric acid treatment, resulting in intercalation of acid molecules between the graphite planes. Thus, graphite intercalation compounds are prepared. On subsequent heat treatment or microwave irradiation, expanded graphite is formed due to bursting of acid molecules, which results in the expansion along the "*c*" direction few hundred times as reported by Chung et al.[29] Further, it is easy to synthesize GNSs from expanded graphite by *ultrasonicating* the latter in a suitable solvent. Hence, compared to graphene and CNT, expanded graphite is a better alternative from the perspectives of cost and ease of synthesis. Hence, in this work, expanded graphite has been used as the filler. The high-aspect-ratio fillers also act as heterogeneous nucleation sites when incorporated in a suitable polymer matrix. Since nanostructures are metastable structures, they are prone to agglomeration which should be avoided. Due to this reason, often surfactants such as cetyltrimethylammonium bromide (CTAB),[30] sodium dodecyl benzenesulfonate,[31] etc., are used to improve the dispersion of the fillers in water or suitable organic solvents. The selection of a surfactant is critically dependent on the filler and polymer matrices chosen. Among various surfactants, polyvinylpyrrolidone (PVP) has been reported to significantly enhance the dispersion of graphite nanostructures due to its high affinity toward the graphite particles when the filler particles are dispersed in organic solvents.[32] Since the present work is related to solution blending of PVDF-ExGr nanocomposites, GNSs are dispersed in the chosen solvent with PVP.

Bentini et al.[33] have studied the thermal stability and oil absorption capacity of the highly porous PVDF-ExGr composite system. However, the authors did not report structure development in that composite system, and the electrical properties correlated to the dispersion of ExGr particles. Xie et al.[34] have analyzed the effect of various surfactants such as CTAB, PVP, and KH-550 on the dispersion characteristics of graphite nanoplatelets in dimethylformamide (DMF) and synthesized PVDF-modified graphite nanoplatelet composites by solution mixing followed by a compression molding technique. The graphite nanoplatelets are bath-sonicated in DMF for more than 1 day before mixing with the polymer. It has been reported by the authors that the electrical conductivity is reduced, although the dispersion of graphite nanoplatelets has been improved. This could be due to the presence of a thick layer of surfactant molecules on the graphite nanoplatelets. Since the authors have employed the solution blending method followed by the compression molding technique for the preparation of composites, the interparticular distance could have been increased, which is the reason for the decrease in the electrical conductivity. Also, the authors did not investigate the structure development, thermal properties, and contact angle analysis of the chosen composite system.

Zhang et al.[35] have studied the electrical and thermoelectric properties of solution-blended PVDF-ExGr composites using ExGr at different volume expansions as the filler. A high electrical conductivity of 883 S/cm and excellent thermoelectric performance with a power factor of 6.79 μW/m K^2 have been reported for the composite with ExGr obtained by thermal induction of expandable graphite at 600 °C. Li et al.[36] have investigated the dielectric properties of the solvent-cast PVDF−GNS composites by functionalizing GNS using two silane coupling agents to enhance the dispersion in the polymer matrix. The composite in the presence of coupling agents at the percolation threshold of 3 wt % GNS exhibits excellent dielectric properties with low dielectric loss. Deng et al.[37] have investigated the electrical and thermal conductivities of the PVDF-ExGr composite by the ball milling process. The enhancement of thermal and electrical conductivities has been reported with an increase in the loading of ExGr.

Kou et al.[38] have reported enhanced dielectric constant and low dielectric loss for PVDF−PVP-coated graphene oxide composites in which enhancement in the dispersion of the filler particles is realized. The authors did not comment on the processing-route-dependent electrical properties, contact angle analysis along with electroactive phase formation, and quantification. The authors *prepared* composites by solution blending followed by hot pressing at 190 °C and reported a reduction in the electrical conductivity with various loadings of PVP (5, 10, 20 wt %). The authors have reported that the electrical conductivity of PVDF−GO composites is decreased with an increase in the loading of PVP when compared to the conductivity of the composites without PVP. It appears that the amount of PVP used is more, and the system seems to be PVDF−PVP−GO blend nanocomposites and a thick coating of PVP layers *might have impeded* the charge transport. Though

https://doi.org/10.1021/acsomega.3c03083
ACS Omega 2024, 9, 178−195

there are reports related to the surfactant-assisted dispersion of carbonaceous nanofillers when incorporated in the polymer matrix,[39] hardly any paper is published related to the enhancement in the electrical conductivity of composite systems in the presence of surfactant molecules. The surfactant amount and processing methods play a significant role in deciding the electrical conductivity of the polymer composite system. Hence, we have performed a systematic study on the enhancement in the dispersion of GNSs with PVP (1 wt %) as the surfactant in the PVDF matrix, *which reduces the* electrical percolation threshold when the solution blending method is employed for the preparation of PVDF-ExGr composites. The novelty of our work lies in the fact that improved dispersion of GNSs in the presence of surfactant molecules enhances electrical conductivity and also results in structure development in PVDF. We are the first to report enhanced electrical conductivity by incorporating surfactant molecules in solution-blended PVDF-ExGr nanocomposite systems. Thermal properties and the effect of processing routes on the electrical conductivity along with water contact angle (WCA) analysis have been reported for the chosen composite system with and without a surfactant. The results corresponding to 1 wt % PVP loading in solution-blended PVDF-ExGr nanocomposites are reported in the present work, and the results are promising for the development of flexible polymer-based nanogenerators and underwater acoustic sensors.

2. EXPERIMENTAL SECTION

2.1. Materials. PVDF (Grade Solef 1006-MFI-30−40 g/10 min at 230 °C/2.16 kg) is obtained from Solvay Solexis, France. Expandable graphite (grade 3772) is provided by Asbury Carbons Inc., USA. *N*,*N*-Dimethylacetamide (DMAc) (AR grade) is acquired from S.D-fine chemicals, India. PVP (average molecular weight 40,000) is procured from Sigma-Aldrich, USA.

2.2. Synthesis of Expanded Graphite. Expanded graphite is synthesized from expandable graphite by microwave irradiation. Commercial expandable graphite of the amount 0.1−0.2 g is taken in an alumina crucible and placed in a domestic microwave oven (model LGMH2342 (LG, India)—output power-800 W). It is irradiated by microwaves generated in the oven for about 10 s, resulting in the formation of fluffy expanded graphite.

2.3. Preparation of Solution-Blended PVDF-ExGr Nanocomposite Films. PVDF-ExGr nanocomposites are prepared by solvent-casting method. The total composite amount is maintained at 1.5 g. PVDF of appropriate quantity is dissolved in 10 mL of DMAc by mechanical stirring using a hot plate kept at 60 °C. An appropriate amount of expanded graphite is separately added to 10 mL of DMAc and probe sonicated using a probe sonicator (ENUP 500 M/C—life-care equipment, India-500 W, frequency 20 ± 2 kHz. Probe sonication has been carried out at 30 W, 20 kHz) until the GNSs are completely dispersed in the solvent. The PVDF solution is then added to this dispersed GNSs in the solvent, and the mixture is probe sonicated for about 20−30 min intermittently. The heat produced during probe sonication is removed by placing the beaker in a cold-water bath, while sonication is carried out. The solution is then poured into a Petri dish and heated at 60 °C until complete evaporation of solvent results (the odor of solvent is subsided). Once the solvent molecules are evaporated, a thin flexible film is formed. The thickness of the solvent-cast film is 0.1 mm. A series of composite films are made by varying the expanded graphite loading (x (wt %) = 0, 0.1, 0.3, 0.5, 1, 1.5, 2, 3) according to the calculation. The samples are designated as the PEG series. PEG0.5 refers to the PVDF-0.5 wt % ExGr nanocomposite without PVP. Similarly, PEG1 refers to PVDF-1 wt % ExGr nanocomposite. (P refers to the first letter of PVDF, EG refers to expanded graphite, and number following EG refers to wt % of filler content.) A neat PVDF film is prepared after dissolving the required amount of PVDF granules in DMAc at 60 °C as mentioned above followed by probe sonicating the solution, and then, it is cast in a Petri dish.

2.4. Preparation of Solution-Blended PVDF-ExGr−PVP Nanocomposite Films. The preparation of solution-blended PVDF-ExGr−PVP films is similar to that of the procedure mentioned in Section 2.3 and is detailed in Supporting Information Section S1.1.

2.5. Preparation of the PVDF-ExGr Nanocomposite Film with and without PVP by Compression Molding. The solvent-cast PVDF-ExGr film with different loadings of filler particles is folded and placed between stainless-steel plates. The steel plates are preheated to a temperature of about 240 °C on a compression molding press [Bharaj BCP 40 (Bharaj Machineries Pvt. Ltd., India)—machine tonnage—40; platen area—1 sq. ft.; maximum mold heater temperature—300 °C]. The film was compressed at a pressure of 170−200 kg/cm^2. The curing time for the film formation is kept at 10 min. The films of PVDF-x wt % ExGr and PVDF-x wt % ExGr-1 wt % PVP nanocomposites with different loadings of ExGr (x wt % = 0, 0.5, 1, 2) are prepared for electrical resistance measurements.

2.6. Characterization Techniques. The electrical characterization, optical microscopy analysis, X-ray diffraction (XRD) analysis (structural characterization), Fourier transform infrared spectroscopy (FTIR) analysis, differential scanning calorimetry (DSC) analysis, thermogravimetric analysis (TGA), field emission scanning electron microscopy (FESEM), and WCA analyses of PVDF-ExGr nanocomposites without and with 1 wt % PVP are detailed in Supporting Information Sections from S2.1 to S2.8, respectively.

3. RESULTS AND DISCUSSION

3.1. Dispersion of Expanded Graphite. The dispersion of expanded graphite in DMAc solvent is investigated with and without the surfactant, PVP. The ExGr particles in DMAc have been probe sonicated, and the stability of GNS dispersion over time is analyzed. The GNSs dispersed in the presence of PVP exhibited good and stable dispersion without any further agglomeration and settlement for about 2 weeks. This is attributed to the strong affinity of PVP toward sonicated ExGr particles. It has been reported that the hydrogen bonding between PVP and reduced graphene oxide (rGO) results in better dispersion of rGO in the nanocomposite.[43] It has been proved that the carbonyl group of PVP interacts with the hydroxyl group on the surface of the graphene oxide, preventing its agglomeration due to the van der Waals force enhancing the dispersion as reported elsewhere.[44] Since, in the present work, expanded graphite has been used, which is obtained by microwave irradiation of expandable graphite (expandable graphite is usually obtained by sulfuric acid/nitric acid intercalation), the presence of functional groups such as hydroxyl groups on the GNSs cannot be ruled out. Hence, PVP can interact well with GNSs. PVP has been proven to effectively disperse high concentration of graphene dispersion

https://doi.org/10.1021/acsomega.3c03083
ACS Omega 2024, 9, 178−195

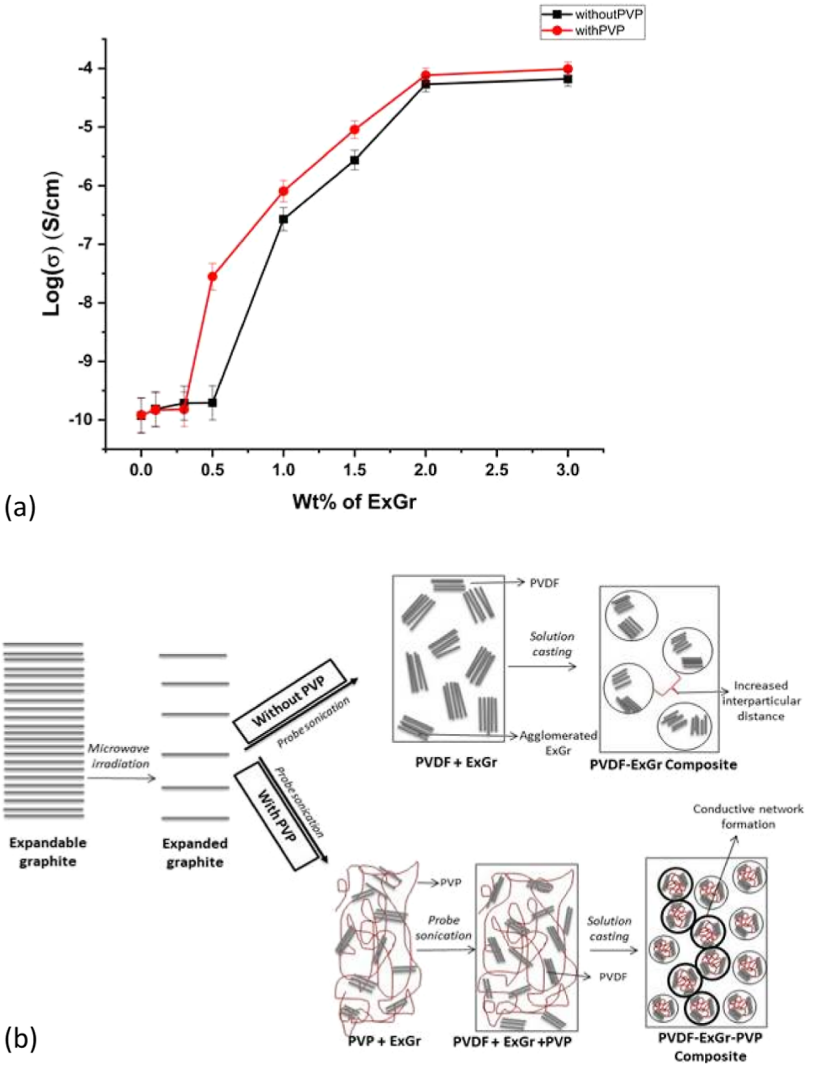

Figure 1. (a) Variation of electrical conductivity in the solvent-cast PVDF-ExGr nanocomposite films with and without PVP. (b) Model depicting the conducting network formation in the PVDF ExGr composites without and with PVP.

in organic solvents and hence act as a stabilizer. PVP prevents reaggregation of graphene layers sterically due to adsorption onto the surface of filler particles as reported elsewhere.[45] Since, in the present work, sonicated expanded graphite in DMAc results in the formation of GNSs, PVP coats onto the filler surface, preventing further agglomeration. Hence, the dispersion of GNSs is improved in DMAc and also in the polymer matrix when solution-blended nanocomposites are prepared. Further, the hydrophobic interaction between PVP and graphene has been reported to be the cause of better dispersion in water as reported by Yoon and In.[46] Similarly, in the presence of CTAB, the dispersion of sonicated ExGr is stable for less than 4 h as observed through the experiments. Hence, compared to CTAB, for the same amount of PVP (1 wt %), the dispersion of GNSs in DMAc is found to be more stable for many hours. The dispersion of the GNSs without PVP is stable for a shorter duration of time comparatively. The settlement of agglomerated GNSs can be seen clearly in less than 6 h. Since PVP has been observed to be very effective in dispersing the GNSs, it is used as the surfactant for this study. The amount of PVP has been fixed at 1 wt % for the preparation of PVDF-ExGr nanocomposites. Thus, PVP has better affinity to GNSs whether chemical interaction exists between them due to the presence of functional groups onto the surface of GNSs or hydrophobic interaction between them. Experimentally, better interaction between PVP and GNSs has been confirmed as the dispersion of GNSs in DMAc stays for a longer duration.

3.2. DC Conductivity Analysis of Solution-Blended PVDF-ExGr Nanocomposites. Figure 1a depicts the non-linear electrical conductivity variation of solvent-cast PVDF-*x* wt % ExGr (*x* = 0, 0.3, 0.5, 1, 1.5, 2, 3) and PVDF-1 wt % PVP-*x* wt % ExGr (*x* = 0, 0.3, 0.5, 1, 1.5, 2, 3) composite films. The electrical conductivity of the PVDF-*x* wt % ExGr-1 wt % PVP nanocomposite system is higher than that of the PVDF-*x* wt % ExGr nanocomposite system. The electrical conductivity of PPEG0.5 is about 2 orders higher than that of PEG0.5. This is due to more uniform distribution of GNSs, which results in better conductive network formation between them in the PVDF matrix on incorporating the surfactant, PVP. The enhanced dispersion of GNSs has reduced the percolation threshold to 0.3 wt % ExGr in the composite system with PVP, as shown in Figure 1a. The composite system without PVP has a *comparatively* higher percolation threshold of 0.5 wt % ExGr due to less dispersed GNSs in the PVDF matrix. When PVP is incorporated, at lower concentration itself, effective network

https://doi.org/10.1021/acsomega.3c03083
ACS Omega 2024, 9, 178−195

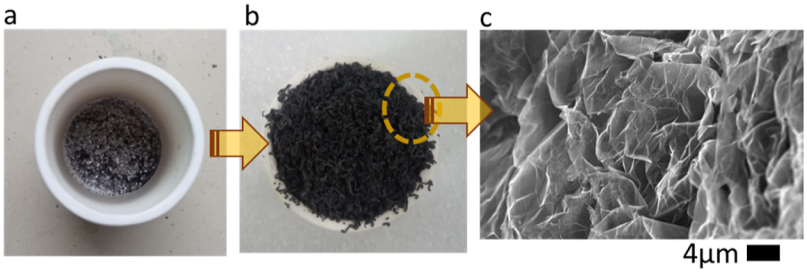

Figure 2. Digital pictures of (a) expandable graphite (before microwave irradiation), (b) expanded graphite (after microwave irradiation), and (c) FESEM micrograph of expanded graphite.

formation between the filler particles could be obtained because of enhanced dispersion in the polymer matrix. This aspect will be proved in FESEM analysis. In fact, optical microscopy images prove the fact that in the *PVDF-ExGr* nanocomposite with PVP, the dispersion of GNSs is better in comparison to the nanocomposite without PVP as explained in Section S3 of the Supporting Information. The variation of electrical conductivity with the loading of ExGr follows the typical percolation behavior. The experimental results confirm the fact that PVP has more affinity toward graphite particles. It should be mentioned that the PEG3 (PVDF-3 wt % ExGr without PVP) film is slightly rougher in comparison to the same composite with 1 wt % PVP. Also, the film formation has been observed to be slightly difficult in comparison to that of PPEG3 due to random distribution of GNSs in PEG3. A model, as depicted in Figure 1b, clearly shows that probe sonication of expanded graphite forms agglomerated GNSs, which on mixing with polymers do not form enough conducting networks at lower loadings because of increased interparticular distance. However, in the presence of PVP, which has more affinity toward GNSs, PVP-encapsulated GNSs reduce the agglomeration. Thus, the number of filler particles increases eventually, resulting in the reduction of the electrical percolation threshold due to more network formation. The electrical conductivity enhancement proves the fact that the coating thickness of PVP onto GNSs will be much less with a possibility of charge transport as the interparticle distance between the fillers is reduced. However, electrical conductivity reduction has been reported with a higher loading of PVP probably due to increased barrier thickness around GO in PVDF.[38] It should be mentioned that when the barrier thickness is less than 50 Å, tunneling conduction is possible. The result of the present investigation suggests that a very thin layer of PVP coating onto the GNSs would have been formed through which charge transport is possible.

3.3. FESEM Analysis. The expanded graphite has been synthesized from commercial expandable graphite by microwave irradiation, as shown in Figure 2a,b. The expandable graphite upon microwave irradiation results in the bursting of intercalated acid molecules, leading to a huge expansion of the graphite layers along the *c*-axis. The FESEM micrograph of ExGr shows a more porous and vermicular structure, as depicted in Figure 2c. When expanded graphite is probe sonicated in a suitable solvent it forms GNSs.

Similarly, the surface morphology of solvent-cast composite films with and without PVP is analyzed. The cross sections of the etched PEG1 and PPEG1 films are shown in Figure 3a,b, respectively, under different magnifications. The rough surface indicates the polymer surface. The micrograph of the PEG1

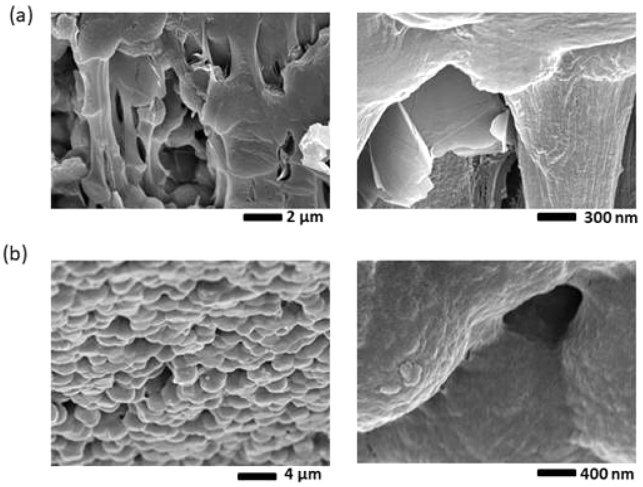

Figure 3. FESEM picture of cross section of the solution-blended (a) PEG1 and (b) PPEG1 nanocomposite films at different magnifications.

film clearly shows the random occupation of agglomerated GNSs in the PVDF matrix, which is a solid proof for the nonuniform distribution of the fillers in the matrix. Clusters of GNSs can be found in a particular region surrounded by thick polymer layers, as depicted in Figure 3a. Since the number of networks between conducting nanofillers is reduced because the filler particles are randomly located, the conductivity of the PVDF-ExGr composite system without PVP is lesser than that of composites with PVP. The FESEM micrograph of the cross-section of etched PPEG1 shows the uniformly arranged GNSs (thickness less than 100 nm), which indeed is an agglomerated structure (as shown in Figure 3b). The orderly arrangement of filler particles coated with PVP is evident from Figure 3b. This is an added proof for the interaction of PVP with ExGr, which has led to more uniform and enhanced dispersion of the fillers in PVDF. It has been proved in the literature that PVP has better interaction with graphene oxide.[43] Since expanded graphite is produced by acid intercalation (sulfuric acid, perchloric acid, etc.) between graphite layers followed by heat treatment at high temperatures or microwave irradiation, the possibility of the existence of carboxyl and hydroxyl functional groups cannot be ruled out, and hence, the interaction between PVP and GNSs can be understood. Further, during solvent casting, since PVDF is a semicrystalline polymer, it would crystallize faster and PVP chains will be wrapping the GNSs. It should be mentioned that PVP is an amorphous polymer. Because of the enhanced dispersion of GNSs due to PVP addition, the contact between filler particles is established at lower loading itself, which results in higher electrical

https://doi.org/10.1021/acsomega.3c03083
ACS Omega 2024, 9, 178−195

conductivity when compared to the conductivity of the composites without PVP. Evidently, the GNSs are agglomerated but uniformly dispersed. The agglomeration of GNSs with PVP is less than what has been observed to be in the absence of PVP. Though PVP coats the agglomerated GNSs, the thickness of the coating decides the charge transport through the system. Excess use of surfactant decreases the electrical conductivity of the nanocomposites as the thickness of the coated layer might increase, which will affect the charge transport. However, our experimental results prove the fact that with incorporation of 1 wt % PVP in PVDF-ExGr composites, better network formation between filler particles results in the enhancement in the electrical conductivity of nanocomposites. The interaction between PVP and ExGr can also be understood through DSC analysis, as discussed in the later sections. It has been proved in this work that there exists a possibility to enhance electrical conductivity at an appropriate loading of PVP in PVDF-ExGr nanocomposites prepared by a solution-blending technique. *It should be mentioned that if phase separation between polymer and filler particles exists, GNSs would have been randomly distributed and agglomerated in the presence of PVP. However, the FESEM result supports uniform distribution of filler particles in the presence of PVP in PVDF and hence phase separation issues would not have resulted.*

3.4. XRD Analysis. Figure 4a shows the XRD patterns of the solution-blended neat PVDF film, ExGr, PPEG0, PPEG0.5, and PPEG1 films, respectively. The major peak of ExGr is observed around 26.5°, which corresponds to the 002 reflection. The solution-cast neat PVDF film exhibits the characteristic gamma phase peaks at 18.5° (002), 20.3° ((110)/(101)) as reported elsewhere.[40] The gamma phase peak of PVDF can be observed in all the composites with and without PVP. On comparing the XRD patterns of neat PVDF with that of the PPEG0 composite, the intensity corresponding to the (110)/(101) reflection of the electroactive gamma phase has been increased, as depicted in Figure 4c, suggesting the interaction between PVP and PVDF such that the crystallite size is increased. This can be attributed to the interaction between the carbonyl groups of PVP and the methylene groups in the PVDF matrix as reported elsewhere.[47] Because of this interaction in a single PVDF chain, the carbon and fluorine atoms arrange such that the gamma crystal configuration is extended. When more chains pack together, this results in crystallite size enhancement. On adding 0.5 wt % ExGr in PVDF with PVP, the intensity of the gamma phase (110)/(101) plane decreases as shown in Figure 4d when compared to that of composites without PVP. This result implies the fact that PVP coils around GNSs, and hence, the interaction between the filler and PVDF is screened. Also, the composite filler can occupy inter-PVDF chains, resulting in a decrease in the peak intensity of the electroactive gamma phase. A similar trend can be seen in Figure 4e in which the XRD patterns of PVDF-1 wt % ExGr with and without PVP are compared. The existence of the gamma phase is confirmed even at the higher loading of ExGr in the composites without PVP. The peak intensity corresponding to the electroactive gamma phase of PVDF with PVP and 1 wt % ExGr loading increases compared to that of 0.5 wt % loading, although the PVDF content is less in the former case, which is a clear indication of the presence of agglomerated GNSs with insufficient coiling of PVP chains due to an enhanced number of GNSs. Thus, a smaller number of GNSs that are not coated well by PVP can interact with PVDF chains enhancing the

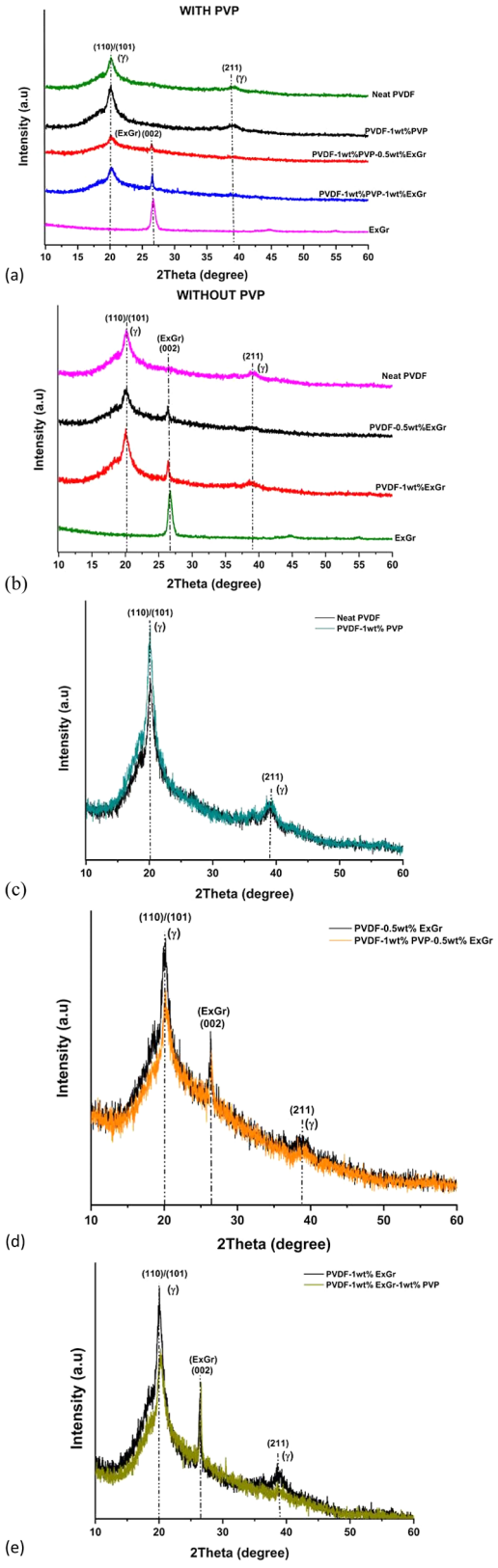

Figure 4. X-ray diffractograms of solvent-cast PVDF-ExGr nanocomposites (a) with PVP and (b) without PVP. Comparison of XRD patterns of (c) neat PVDF and PVDF-1 wt % PVP films, (d) PVDF-0.5 wt % ExGr films with and without PVP, and (e) PVDF-1 wt % ExGr films with and without PVP.

https://doi.org/10.1021/acsomega.3c03083
ACS Omega 2024, 9, 178−195

electroactive phase configuration in PVDF chains when compared to that of 0.5 wt % ExGr loading with PVP. In fact, the XRD of PVDF-ExGr without PVP results in enhanced intensity from planes corresponding to the electroactive gamma phase due to the absence of PVP. Though the crystallize size can be correlated with the intensity enhancement of the gamma phase (from the peak at 20.3° alone), the percentage of crystallinity cannot be commented upon as the latter parameter is related to the area under all the gamma phase peaks in XRD. Actual crystallinity calculation will be done through DSC analysis, and the gamma phase fraction calculation will be done through FTIR analysis. The following conclusion can be arrived at from the XRD analysis of PVDF-ExGr nanocomposites.

1. PVP has better interaction with GNSs.
2. Without PVP, GNSs have better interaction with PVDF chains.

Figure 4b depicts the XRD patterns of the neat PVDF film, ExGr, PEG0.5, and PEG1 composite films, respectively. These composites without PVP also exhibit the characteristic peak of the gamma phase (110)/(101) of PVDF. The peak intensity corresponding to the electroactive gamma phase reflection in the PEG1 composite is higher than that of the PEG0.5 composite despite the reduction in polymer content in the former composite. This result suggests that sonicated ExGr particles can induce electroactive phase due to the interaction between π-electrons in GNSs and the $-CF_2$ groups in PVDF as reported elsewhere.[48] Compared to the peak intensity corresponding to the (110)/(101) reflection of the gamma phase of the solvent-cast neat PVDF film, the peak intensity of the same reflection in PVDF-0.5 wt % ExGr composites is reduced. However, when 1 wt % ExGr is incorporated in PVDF, the peak intensity corresponding to the (110)/(101) reflection is increased in comparison to that of the neat PVDF film. This result also confirms the fact that GNSs can induce a more electroactive gamma phase. It should be mentioned that the full width at half-maximum (fwhm) of the 1 wt % ExGr-loaded composite corresponding to the electroactive gamma phase as shown in Table 1 is reduced in comparison to that of neat PVDF and PVDF-0.5 wt % ExGr composite films. Thus, the crystallite size of the electroactive phase of PVDF is increased with an increase in the loading of ExGr up to 1 wt % in PVDF. This can be attributed to the fact that GNSs can induce more electroactive phase in a PVDF chain due to better interaction. This would have increased the crystallite size when the other chains come closer. Though the crystallite size corresponding to the electroactive gamma phase increases with the loading of 0.5 wt % ExGr in PVDF when compared to that in the neat PVDF film (as the fwhm decreases for the composite), the peak intensity is reduced because GNSs would have been randomly distributed in the polymer matrix, as evidenced in FESEM analysis, and the total number of gamma crystals of PVDF would have been effectively reduced. In a way, the crystallite size locally increases due to incorporation of ExGr into the polymer matrix. As mentioned before, from the peak intensity, crystallinity cannot be commented upon. However, the variation of peak intensity becomes a proof for the interaction of GNSs with PVDF chains.

Table 1. Comparison of fwhm and Peak Intensity Variation in Solution-Blended PVDF-ExGr Nanocomposite Films with and without PVP

composition	peak intensity of gamma phase reflection (110)/(101) [20.3°]	fwhm [deg]
	without PVP	
PEG0	786	0.8160
PEG0.5	652	0.8029
PEG1	868	0.5353
	with PVP	
PPEG0	1021	0.8129
PPEG0.5	552	0.8060
PPEG1	681	0.6691

The solvent plays a major role in the generation of the electroactive phase in the neat PVDF film. In short, through XRD, it is confirmed that in solution-blended PVDF-ExGr nanocomposites with and without PVP, the electroactive gamma phase is generated, which exhibits compositional dependence, i.e., on the loading of ExGr. The interaction between PVP and GNSs, along with PVDF chains and GNSs, can be qualitatively understood from the XRD results.

3.5. FTIR Analysis. The FTIR spectra of solution-blended neat PVP, PPEG0, PPEG0.5, and PPEG1 films are shown in Figure 5a and that of PEG0, PEG0.5, and PEG1 are shown in

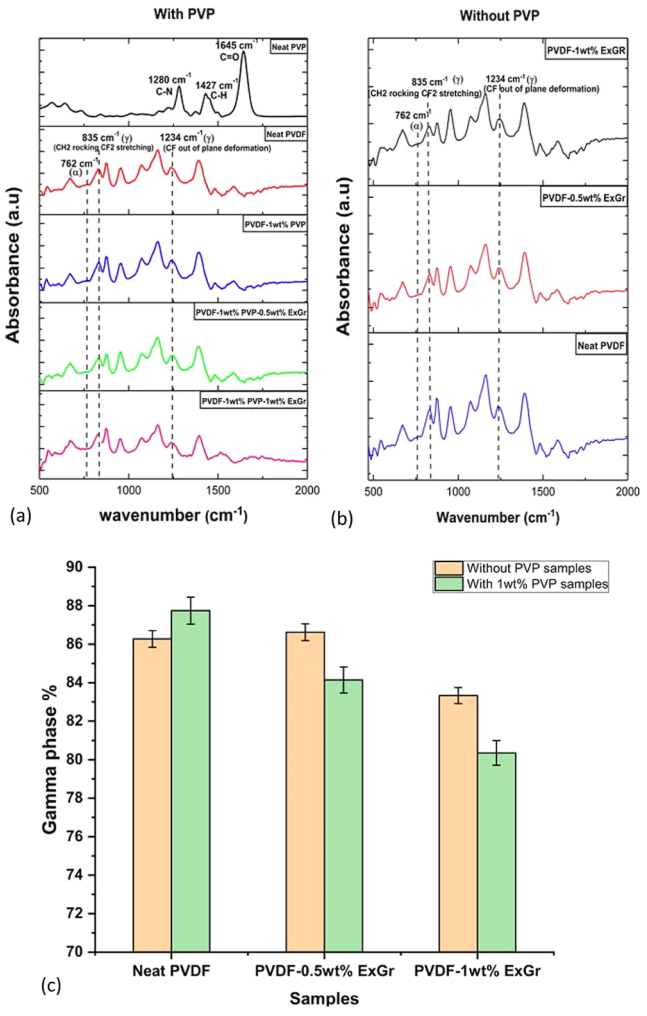

Figure 5. FTIR of spectra of solvent-cast samples (a) with PVP (neat PVP, neat PVDF, PPEG0, PPEG0.5, PPEG1) and (b) without PVP (neat PVDF, PEG0.5, PEG1). (c) Electroactive gamma phase content in the solution-blended PVDF-ExGr nanocomposite film with and without 1 wt % PVP.

https://doi.org/10.1021/acsomega.3c03083
ACS Omega 2024, 9, 178−195

Figure 5b. The existence of the electroactive gamma phase is confirmed in the neat PVDF film itself due to the presence of vibration bands at 833 cm^{-1} (CH_2 rocking) and 1234 cm^{-1} (CF_2 out-of-plane deformation) as reported elsewhere.[49] The incorporation of ExGr does not affect the gamma crystal structure in the PVDF-ExGr composites with and without PVP. The confirmatory bands of the gamma phase of PVDF are seen in all samples. There are also a few alpha phase vibration bands observed at 540 cm^{-1} (CF_2 bending), 762 cm^{-1} (very weak), and 1388 cm^{-1} in PEG0 and PPEG0. PEG1 has alpha phase vibration bands around 762 cm^{-1} (very weak), 871 cm^{-1} (CH out-of-plane deformation), and 1388 cm^{-1}. PPEG1 exhibits alpha phase vibration bands around 547 and 1388 cm^{-1}. The coexistence of alpha and electroactive gamma phases in all of the composites has been proved by FTIR analysis. Since neat PVDF also exhibits an electroactive gamma phase, it is to be mentioned that the solvent has a great role in the phase transformation in PVDF. It should also be mentioned that the vibration bands corresponding to PVP do not interfere with the confirmatory vibration bands of the electroactive gamma phase of PVDF.

Figure 5c shows the comparison of the electroactive phase content in solution-blended PVDF-ExGr nanocomposites with and without PVP for selected samples. The electroactive gamma phase of PVDF increases with 1 wt % PVP incorporation, suggesting better interaction between PVP and PVDF. The gamma phase content of the neat PVDF film (86.2%) has been increased to 87.2% in the PEG1 film. Also, with the incorporation of 0.5 wt % expanded graphite without PVP, a slight increase in gamma phase content has been realized (86.6%). This is attributed to the interaction between π-electrons of GNSs and the CF_2 dipoles in PVDF as reported elsewhere.[48] Since the network formation is initiated at that loading of ExGr (0.5 wt %), there can be more filler edges that could have been exposed, resulting in a slight increase in the electroactive phase. When the ExGr loading is increased to 1 wt %, a decrease in gamma phase content (83.3%) is realized. Since this loading is above the percolation threshold, there will be more network formation between GNSs so that a smaller number of filler edges would be exposed to the polymer matrix, and hence, the electroactive phase content in the nanocomposite is decreased. However, the electrical conductivity is enhanced due to the network formation between the fillers. This kind of result has been published elsewhere.[50] Also, the filler particles can occupy inter-PVDF chains, affecting the crystallinity. It should be mentioned that the DSC analysis proves the fact that crystallinity is decreased when 1 wt % ExGr is incorporated into the PVDF matrix when compared to that of the neat PVDF film.

When 1 wt % PVP is incorporated into PVDF-x wt % ExGr (x = 0.5, 1) composites, the fraction of the gamma phase of PVDF is decreased in comparison to the composites without PVP. This is attributed to the fact that PVP coils around GNSs due to the crystallization of PVDF from the solution, while the solvent is removed, which makes PVP chains adhere onto GNSs. It must be noted that PVP incorporation resulted in better dispersion of GNSs in the polymer matrix, as evidenced by the FESEM pictures. Hence, more composite fillers can occupy inter-PVDF chains, affecting both crystallinity and the electroactive phase content. The interaction of GNSs with PVDF chains is hindered because of PVP wrapping, and hence, the electroactive gamma phase content is less compared to that of the composites without PVP with the same loading of filler particles. Table.2 depicts the variation in the gamma phase content concerning filler loading for solution-blended samples.

Table 2. Gamma Phase Content Variation in Solution-Blended PVDF-ExGr Films with and without PVP

	electroactive gamma phase content (%) [solvent casting]	
sample	with 1 wt % PVP	without PVP
PEG0	87.74 ± 1.16	86.27 ± 1.63
PEG0.5	84.14 ± 0.86	86.62 ± 1.38
PEG1	80.35 ± 0.65	83.33 ± 1.47

3.6. DSC Analysis. Figure 6a depicts the melting DSC curves of solution-blended PVDF-x wt % ExGr (x = 0, 1, 2) with and without PVP. It can be seen that there are two melting peaks fused in both systems with and without PVP at 1 wt % ExGr and 2 wt % ExGr loadings in PVDF. The higher temperature melting peak (170−174 °C) corresponds to the gamma phase of PVDF, and the lower temperature melting peak (∼165−169 °C) corresponds to the alpha phase of PVDF as cited in the literature.[41,42] Figure 6b shows the crystallization peaks of PVDF-ExGr nanocomposites with and without PVP. To explicitly show two melting peaks, the deconvoluted melting peaks of representative samples are depicted in Figure S3a−c in Section S4 of Supporting Information. The deconvolutions are done using the Voight function. It can be seen from Table S1 (Supporting Information) that the area under the high-temperature melting peak (corresponding to the gamma phase) is increased from neat PVDF to PPEG0, signifying an increase in the gamma phase content. Also, the area under the low-temperature melting peak is reduced when 1 wt % PVP is incorporated in PVDF, suggesting that the alpha phase content is reduced compared to that of neat PVDF. Similarly, for PPEG1, the area under the high-temperature melting peak is less than that of the neat PVDF and PPEG0, signifying that the electroactive gamma phase content is reduced. Also, the area under the alpha phase melting peak is increased, suggesting higher alpha phase content when compared to that of neat PVDF and PPEG0. The ratio of the area under the gamma phase to the area under the alpha phase (A_γ/A_α) melting curves for the selected samples follows the crystallinity data as shown in Table S1 (in Supporting Information). The trend in the variation in areas corresponding to the phases of PVDF is consistent with the FTIR analysis discussed earlier. In short, deconvolution of the melting peaks corresponding to PVDF-ExGr nanocomposites with and without PVP proves the coexistence of nonpolar alpha and electroactive gamma phases, and variation in the electroactive phase in the composites is consistent with FTIR analysis.

The XRD data also support the existence of the gamma phase in both composite systems with and without PVP. The crystallinity calculated using the enthalpy corresponding to the melting peak is tabulated in Table 3. From the data, the percentage crystallinity of neat PVDF is around 40.79, and when 1 wt % PVP is incorporated in PVDF, it increases to 56.5. Also, the crystallization temperature has been shifted to a higher temperature. This indicates that PVP acts as a nucleating agent. This is due to the interaction between the PVP and the PVDF chains as cited elsewhere.[51] The melting temperature of PPEG0 is higher than that of neat PVDF, which also indicates that there should be an interaction between

https://doi.org/10.1021/acsomega.3c03083
ACS Omega 2024, 9, 178−195

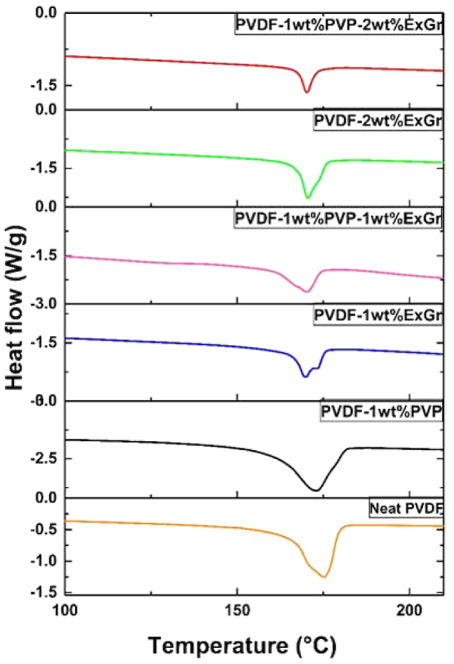

(a)

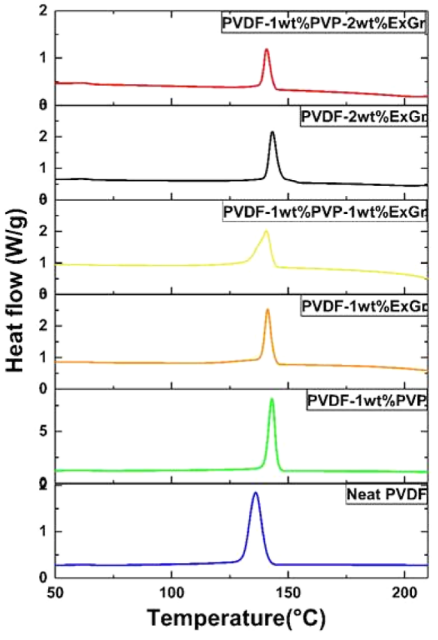

(b)

Figure 6. DSC curves of solution-cast PVDF-x wt % ExGr (x = 0, 1, 2) with and without PVP: (a) melting curves and (b) cooling curves.

PVDF and PVP. In the PPEG1 sample, the percentage crystallinity has been reduced to 30.02. This shows that PVP has more affinity toward GNSs and gets coated onto the filler's surface reducing its exposure to the PVDF matrix. Also, PVP-coated GNSs can act as a separator between PVDF chains, which results in a decrease in the crystallinity. This fact is also proven for PPEG2 composites. More sonicated expanded graphite particles result in GNSs, which can act as separators between the PVDF chains, resulting in lesser crystallinity. The percentage crystallinity is reduced from 30.02 for 1 wt % ExGr in PVDF with 1 wt % PVP to 12 for 2 wt % ExGr in PVDF with 1 wt % PVP. The DSC results strongly support the fact that the interaction of PVP is stronger with GNSs than that of PVDF. It is due to this interaction that the dispersion of GNSs is found to be better in the polymer matrix, as evidenced through FESEM analysis of the composites.

In the case of PEG1, the crystallinity is 31.73%, which is a little higher than that of PPEG1. At 1 wt % loading of ExGr, the crystallinity is decreased in comparison to that of neat PVDF because of the occupation of filler particles in between PVDF chains apart from the fact that network formation between them would have occurred. Due to the occupation of GNSs in the interspace of PVDF chains, the polymer chains cannot come closer, resulting in lesser crystallinity. The crystallization temperature has been observed to be decreased compared to that of neat PVDF for the same reason. For PEG2, the crystallinity is 31.8%, which is slightly higher than that of 1 wt % ExGr loading in PVDF. However, an increase in crystallization temperature by almost 1.5 °C can be noticed in comparison to that of neat PVDF. Since at 2 wt % ExGr loading in PVDF, agglomeration could have resulted, compared to 1 wt % ExGr loading in PVDF, there is a possibility of distribution of GNS particles in the polymer matrix which could have come out of the interspace of PVDF chains forming agglomeration with other nanosheets, thereby increasing the crystallization temperature. Thus, the GNSs act as heterogeneous nucleation sites depending on the loading of the filler particles in the polymer matrix (as the crystallization temperature is increased). The melting temperatures of PEG1 and PEG2 are decreased in comparison to that of neat PVDF due to the rapid heat transfer to the polymer matrix through conducting GNSs. PPEG1 has a lower melting point than PPEG0, suggesting enhanced dispersion of PVP-coated GNSs in the former case as the heat transfer is much faster when compared to that of PPEG0. Also, it should be noted that the melting temperature of PEG1 is higher than that of PPEG1, suggesting a better dispersion of GNSs in the latter case. This result also proves the fact that the coating of PVP will be very thin on the surface of the GNSs. Thus, these results do support the electrical conductivity data that the enhancement of dispersion of GNSs coated with PVP chains reduces the

Table 3. Comparison of Melting Temperature, Crystallization Temperature, and Percentage Crystallinity in Solution-Cast Samples with and without PVP

sample	ΔH_m (J/g)	T_m (°C)	ΔH_c (J/g)	T_c (°C)	crystallinity (X_c)= ($\Delta H_m/\Delta H_{m100}$) × 100 (%)
PEG0	42.63	172.85	50.92	141.74	40.79
PPEG0	58.46	173.14	57.81	143.08	56.50
PPEG1	31.06	170.43	46.27	141.07	30.02
PPEG2	12.29	170.25	17.22	140.78	12.00
PEG1	32.83	172.43	33.08	141.21	31.73
PEG2	32.57	170.58	32.57	143.24	31.80

https://doi.org/10.1021/acsomega.3c03083
ACS Omega 2024, 9, 178−195

percolation threshold. The DSC analysis supports the fact that there is a strong interaction between PVP and GNSs. Further, PVP and ExGr particles can act as nucleating agents in improving the crystallinity of the PVDF matrix.

3.7. Thermogravimetric Analysis. Figure 7a shows the TGA curves of ExGr particles, neat PVP, PEG0 (neat PVDF), PEG1(PVDF-1 wt % ExGr), and PPEG1(PVDF-1 wt % ExGr-1 wt % PVP) solution-blended films. Two-step degradation can be observed for neat PVP. *Initially, there is weight loss up to 100 °C, which is due to the evaporation of adsorbed moisture as PVP is hydrophilic.*[52,53] At around 380 °C, the onset degradation of the main chains of PVP occurs. The mechanism of the thermal degradation of PVP is due to its depolymerization to the monomer chain as reported by Loria-Bastarrachea et al.[54] The authors have also reported that there could be a simultaneous reaction yielding oligomers. PVDF exhibits single-step thermal degradation, and the onset of thermal degradation of the main chain is at 438 °C as reported elsewhere.[55] The char content is different at different temperatures above 500 °C. It has been reported in the literature that hydrogen fluoride gas (HF) is the major decomposition product of PVDF. The formation of HF results in a cross-linked structure that cannot be decomposed easily, resulting in increased char content.[56] The mechanisms of degradation of PVDF carbon−hydrogen scission and backbone scission have been well explained by De Jesus Silva et al.[57]

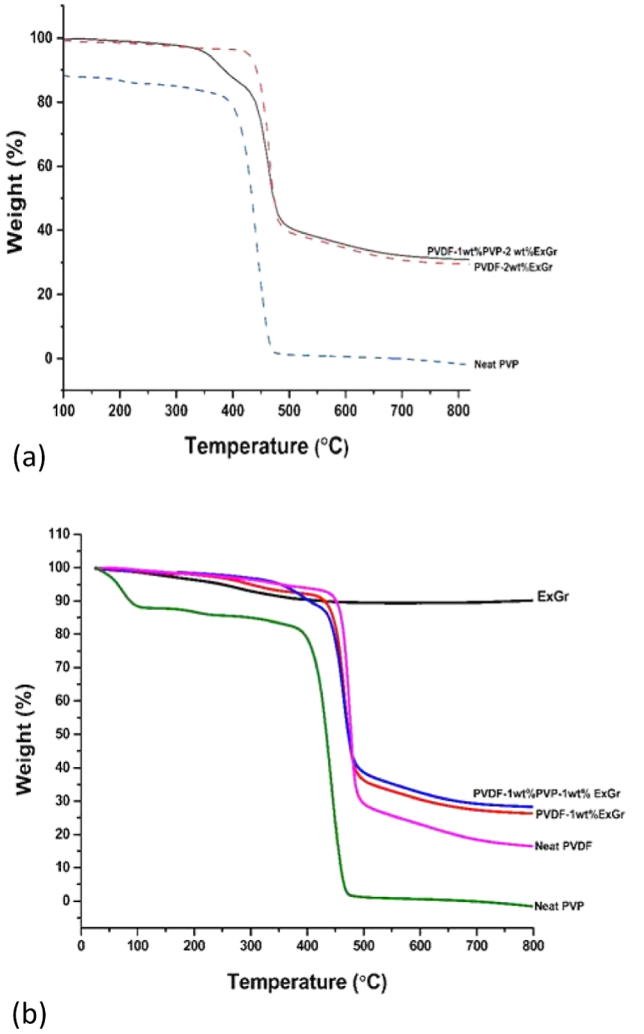

Figure 7. TGA thermograms of (a) ExGr particles, PPEG1, PEG1, neat PVDF, neat PVP films (from top to bottom) and (b) PPEG2, PEG2, and neat PVP films (from top to bottom).

The char content varies with loadings of ExGr and temperatures above 500 °C. The data on the variation of char content are presented in Table 4. TGA of ExGr shows an initial weight loss of about 9%, which is due to the evaporation of moisture adsorbed. TGA can be analyzed in two different regions: above and below 480 °C. Below 366 °C, PPEG1 is more stable than PEG1. This indicates that PVP is coated onto the sonicated ExGr particles preventing the evaporation of volatile contents. Below 366 °C, the heat transfer from ExGr is quite faster, resulting in faster degradation of PEG1. The same reason is valid after 366 °C until 470 °C. A similar interpretation has been cited for RGO−PVP composites.[43] Above 480 °C, the char content for PPEG1 is higher than that for PPEG0, which is attributed to the enhanced dispersion of GNSs as PVP is almost degraded at this stage. PPEG1 has higher char content than neat PVDF and PEG1, as evidenced from Table 4. Because of the uniform dispersion of GNSs and the tortuous pathways created by the filler particles, physical barrier effect is introduced for the thermal degradation and the mobility of degradable products as mentioned elsewhere.[58] Therefore, the char content is higher. Thus, the role of PVP is to enhance the dispersion of GNSs in the PVDF matrix, which results in higher char content. With respect to neat PVP, all nanocomposites exhibit a higher onset thermal degradation. Similar degradation behavior is observed at 2 wt % ExGr loading in PVDF with and without PVP. PPEG2 has higher char content than PEG2, indicating improved dispersion of GNSs. These data support the electrical conductivity data as the electrical conductivity is enhanced due to the dispersion of fillers in the matrix. A similar trend is observed at 2 wt % ExGr loading in PVDF both with and without PVP, as shown in Figure 7b. The char content is different at different temperatures for neat PVDF and the PVDF-1 wt % ExGr composite with and without 1 wt % PVP. However, from Table 4, it can be easily seen that in the presence of PVP, the char content at different temperatures evaluated is higher, which supports the fact that PVP enhances the dispersion of GNSs corroborating the electrical conductivity data. In short, TGA of PVDF-ExGr nanocomposites with and without PVP suggest the following.

1. PVP enhances the dispersion of GNSs in the polymer matrix.
2. Well-dispersed GNSs prevent weight loss and enhance residual char content.

Table 4. Variation of Char Content with Respect to Temperature in Solution-Blended Neat PVDF, PEG1, and PPEG1 Composite Films

	char content (%)		
temperature (°C)	PEG0	PEG1	PPEG1
500	28	36	38
550	25.7	32	35
600	22	30	32
650	20	28	30
700	18	27	29
750	17	26.7	28.7
800	16	26.3	28.4

https://doi.org/10.1021/acsomega.3c03083
ACS Omega 2024, 9, 178−195

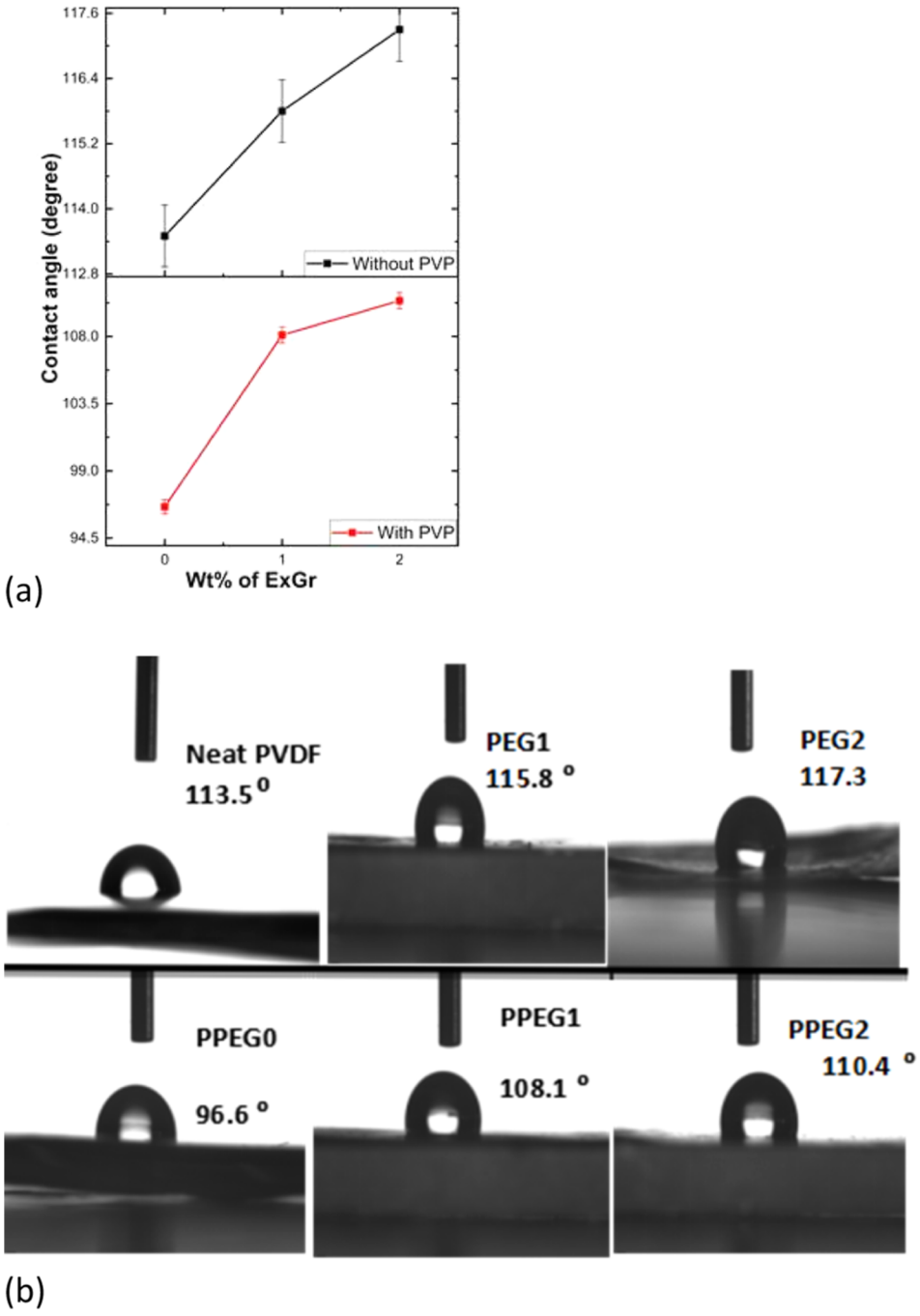

Figure 8. (a) Variation of contact angles of solution-blended PVDF-*x* wt % ExGr (*x* = 0, 1, 2) without and with 1 wt % PVP vs ExGr loading. (b) Digital pictures depicting contact angles of solvent-cast samples: (from top left) neat PVDF, PEG1, PEG2, PPEG0, PPEG1, and PPEG2 composite films.

3.8. Wetting Property Analysis of Solution-Blended PVDF-ExGr Nanocomposites with and without PVP. The variation of contact angle solution-blended neat PVDF, PEG1, PEG2, PPEG0, PPEG1, and PPEG2 composite films is shown in Figure 8a. As observed from the plot, the contact angles of both composite systems (with and without PVP) increase with an increase in ExGr loading. The results indicate an increase in the hydrophobic nature of the composite films with the addition of ExGr to the PVDF matrix. The contact angle of the bare PVDF film is 113.5°, as shown in Figure 8b. It is observed that depending on the preparation route, the contact angle of the same polymer film can be varied as the crystallinity could be different, which might result in different surface roughnesses. Upon the addition of 1 wt % ExGr in PVDF, the contact angle increases to 115.8° and further increases to 117.3° at 2 wt % of ExGr in comparison to that of the neat PVDF film. The increase in contact angle with ExGr loading could be attributed to enhanced surface roughness, which can be explained by the Cassie−Baxter model.[59,60] In the case of the PVDF-ExGr composite system, probe sonication of ExGr in DMAc leads to the formation of GNSs, which results in decreased interparticular distance in the polymer matrix with an increase in the loading of ExGr particles. Therefore, wetting decreased eventually. It should be mentioned that the loading

https://doi.org/10.1021/acsomega.3c03083
ACS Omega 2024, 9, 178−195

of ExGr chosen for the contact angle analysis study is above the electrical percolation threshold of PVDF-ExGr nanocomposites. Similarly, in the case of PVDF-ExGr-1 wt % PVP systems, the contact angle increases with the increase in ExGr loading. However, the contact angles of the PVP-incorporated composite system are less than that of the composite system without PVP, which is attributed to the hydrophilic nature of PVP. The contact angle of PPEG0 is 96.6°, which is less than that of neat PVDF. At 1 and 2 wt % ExGr loadings with PVP in PVDF, the contact angles have been increased to 108.1 and 110.4°, respectively. Despite the addition of PVP, these composites show an increase in contact angle due to the reduced interparticle distance of fillers. Though the contact angle is increased with ExGr loading with PVP, those values are still less than those of the composites with the same loading of ExGr in PVDF without PVP. The surface roughness of the PVDF-ExGr surface would have been increased, as witnessed in the FESEM analysis. A similar analysis has been reported in the literature[61] as well. PVP has strong interaction with GNSs, which results in a more uniform distribution, resulting in a decrease in the interparticular distance. However, the hydrophilic nature of PVP decreases the contact angle of the PVDF-ExGr−PVP nanocomposites. For neat PVDF, with an alpha phase, the contact angle reported is usually around 90°.[62] In our case, for the neat solution-processed PVDF film, the WCA is around 113.5°, suggesting the possibility of the electroactive phase formation, especially the gamma phase. Since the fraction of the gamma phase is higher and the gamma crystals of PVDF are smaller in size,[63] the contact angle could have been increased because of surface roughness variation. It has also been observed that probe sonication of neat PVDF for different times results in variation in the contact angle. However, a separate study in that regard needs to be carried out to analyze the effect of crystallinity variation on the contact angle of the composites.

3.9. Effect of Processing Routes on the Electrical and Wetting Properties of the PVDF-ExGr Nanocomposites.

3.9.1. DC Conductivity Analysis. Figure 9a,b shows the comparison of electrical conductivity variation between the solvent-cast and compression-molded PVDF-*x* wt % ExGr (*x* = 0.5, 1, 2) composites with 1 wt % PVP and without PVP, respectively. The conductivities of PVDF-ExGr composites with and without PVP are comparatively higher for the solvent-cast composites than for the compression-molded samples. This reflects the fact that the processing route influences the conducting behavior of composites. The decrease in electrical conductivity in compression molded samples is due to decrease in the melt viscosity of the polymer which results in the random distribution of the GNSs in the PVDF matrix. Hence, the interparticular distance of GNSs is increased because of the reduction in the melt viscosity. A similar trend is observed in the compression molded composites with PVP also.

3.9.2. XRD Analysis of Compression-Molded PVDF-ExGr Nanocomposites. Figure 10a shows the XRD patterns of compression-molded PPEG0 and PPEG1 composites. Similarly, Figure 10b shows the XRD patterns of compression-molded neat PVDF and PEG1 composites. The XRD patterns of compression-molded samples with and without PVP prove the existence of the electroactive gamma phase of PVDF at 2θ values at 20.3 and 39°, respectively. The enhancement of the alpha phase peak is also observed at 36° for all the samples.[40] In comparison to the solvent-cast samples, the gamma phase

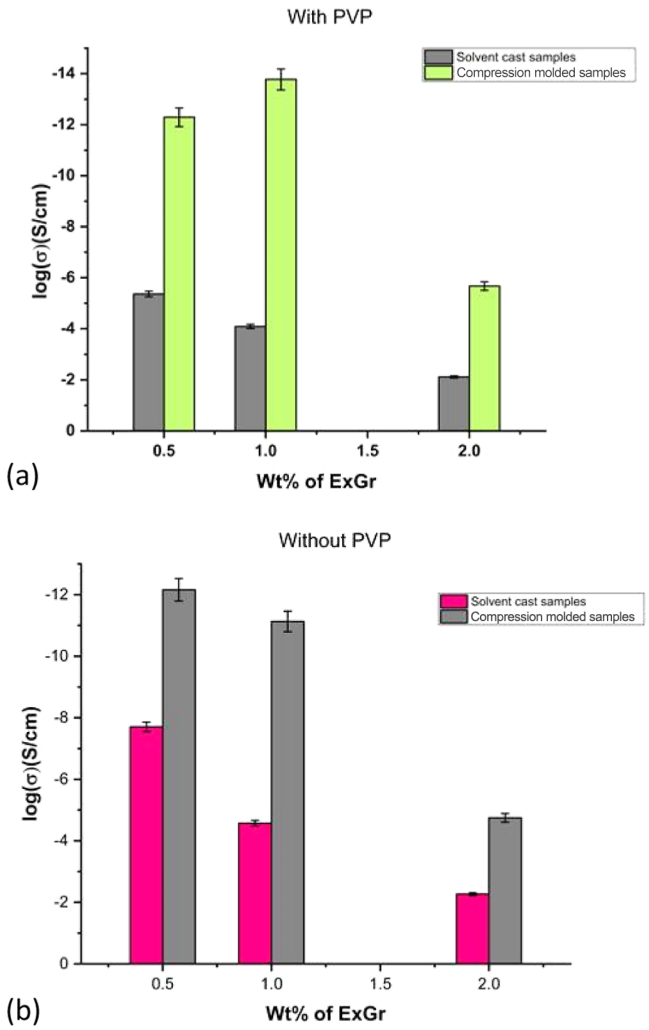

Figure 9. Comparison of electrical conductivities of solvent-cast and compression-molded PVDF-*x* wt % ExGr (*x* = 0.5, 1, 2) composites (a) with 1 wt % PVP and (b) without PVP.

intensity of the compression-molded samples has been considerably increased. The peaks corresponding to the electroactive gamma phase (110/101) are narrow with lower fwhm, indicating the increased crystallite size of the gamma crystals. The peak intensity of graphite at 26.5° (002) has increased comparatively. In composite films with PVP, the enhancement in the peak intensity of planes corresponding to the gamma phase of PVDF can be due to the removal of the PVP coating from the graphite particles. Since the compression molding is carried out at 240 °C, the interaction between graphite and PVP would break, resulting in the removal of PVP coating from the graphite surface. Now, more graphite layers are exposed, and this can result in agglomeration; hence, the peak intensity of the (002) reflection of graphite increases. This also aids in explaining the decrease in the conductivity of the compression-molded samples compared to that of the solvent-cast samples. Similarly, compression molding of PVDF-ExGr composites without PVP at higher temperatures results in a decrease in the melt viscosity of the polymer. This, in turn, would increase the separation of GNSs in the PVDF matrix, making it difficult for better charge transport, and hence, the conductivity is decreased. From electrical conductivity and XRD data of compression-molded composites, it can be

https://doi.org/10.1021/acsomega.3c03083
ACS Omega 2024, 9, 178−195

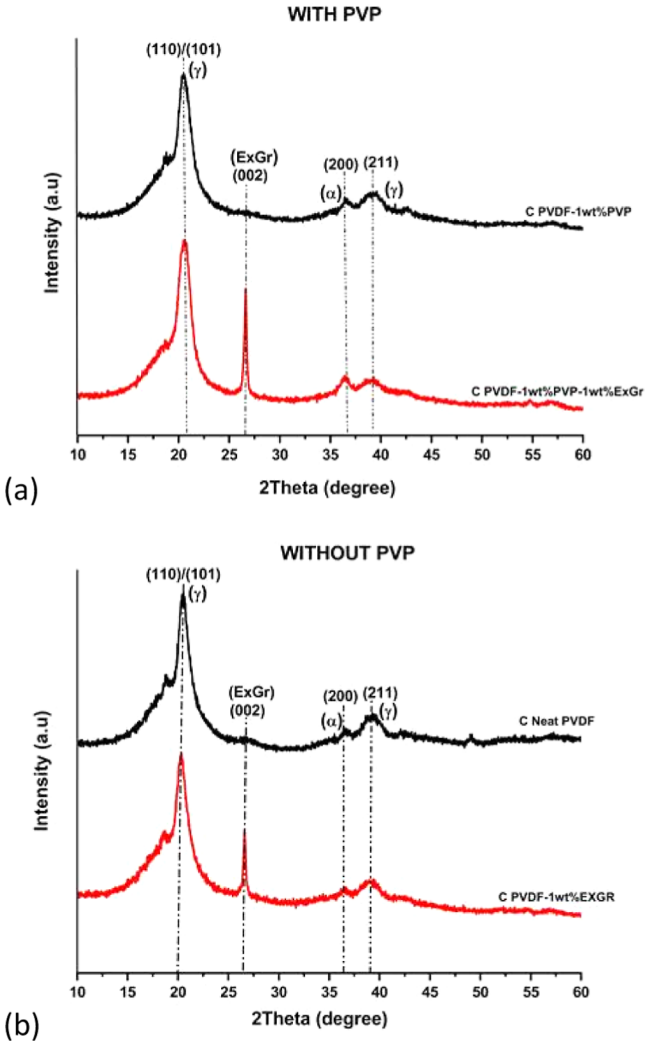

Figure 10. XRD patterns of compression-molded (a) PPEG0, PPEG1 and (b) neat PVDF, PEG1 composite films.

concluded that agglomeration of GNSs occurs at higher loading in PVDF. This brings out the fact that the processing route plays an important role in influencing the crystal phase of the composite film.

3.9.3. FTIR Analysis of Compression-Molded PVDF-ExGr Nanocomposites. The FTIR vibration spectra of the compression-molded PPEG0 and PPEG1 composites are shown in Figure 11a and those of the neat PVDF and PEG1 composites are shown in Figure 11b, respectively. The existence of an electroactive gamma phase is confirmed by the presence of absorption bands at 833 and 1234 cm $^{-1}$ in a compression-molded neat PVDF sheet. The above result proves the fact that the processing conditions have not affected the crystal structure much. Also, vibration bands corresponding to the alpha phase exist like that of the solvent-cast samples. In short, FTIR analysis confirms the existence of electroactive gamma and nonpolar alpha phases in compression-molded samples supporting the XRD results.

The electroactive gamma phase in selected compression-molded PVDF-*x* wt % ExGr (*x* = 0, 1) with and without PVP has been calculated from FTIR vibration bands as already mentioned in Section 2.5. The variation of the electroactive phase with the composition is depicted in Figure 11c. It can be observed that the electroactive gamma phase of PVDF is

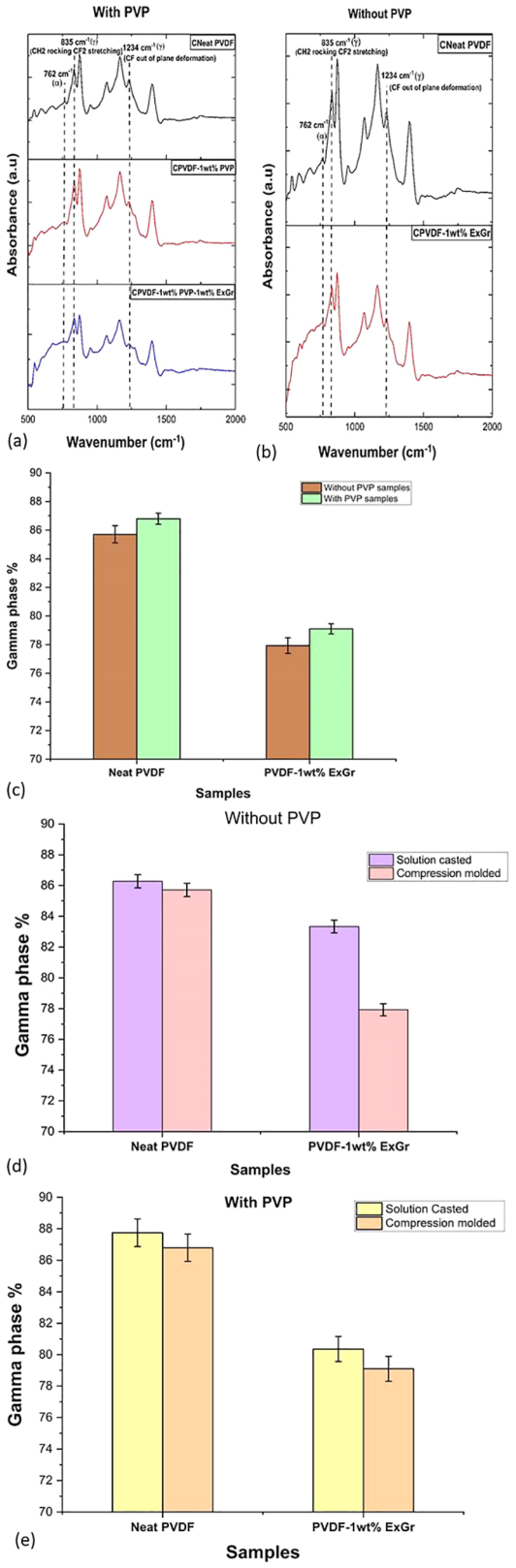

Figure 11. FTIR spectra of compression-molded samples: (a) PPEG0, PPEG1 and (b) neat PVDF, PEG1. (c) Gamma phase variation in compression-molded PVDF-*x* wt % ExGr (*x* = 0, 1) sheets with and without PVP. Comparison of the electroactive gamma phase of the PVDF-ExGr composite prepared by both solution blending and compression molding techniques (d) without PVP and (e) with 1 wt % PVP.

https://doi.org/10.1021/acsomega.3c03083
ACS Omega 2024, 9, 178−195

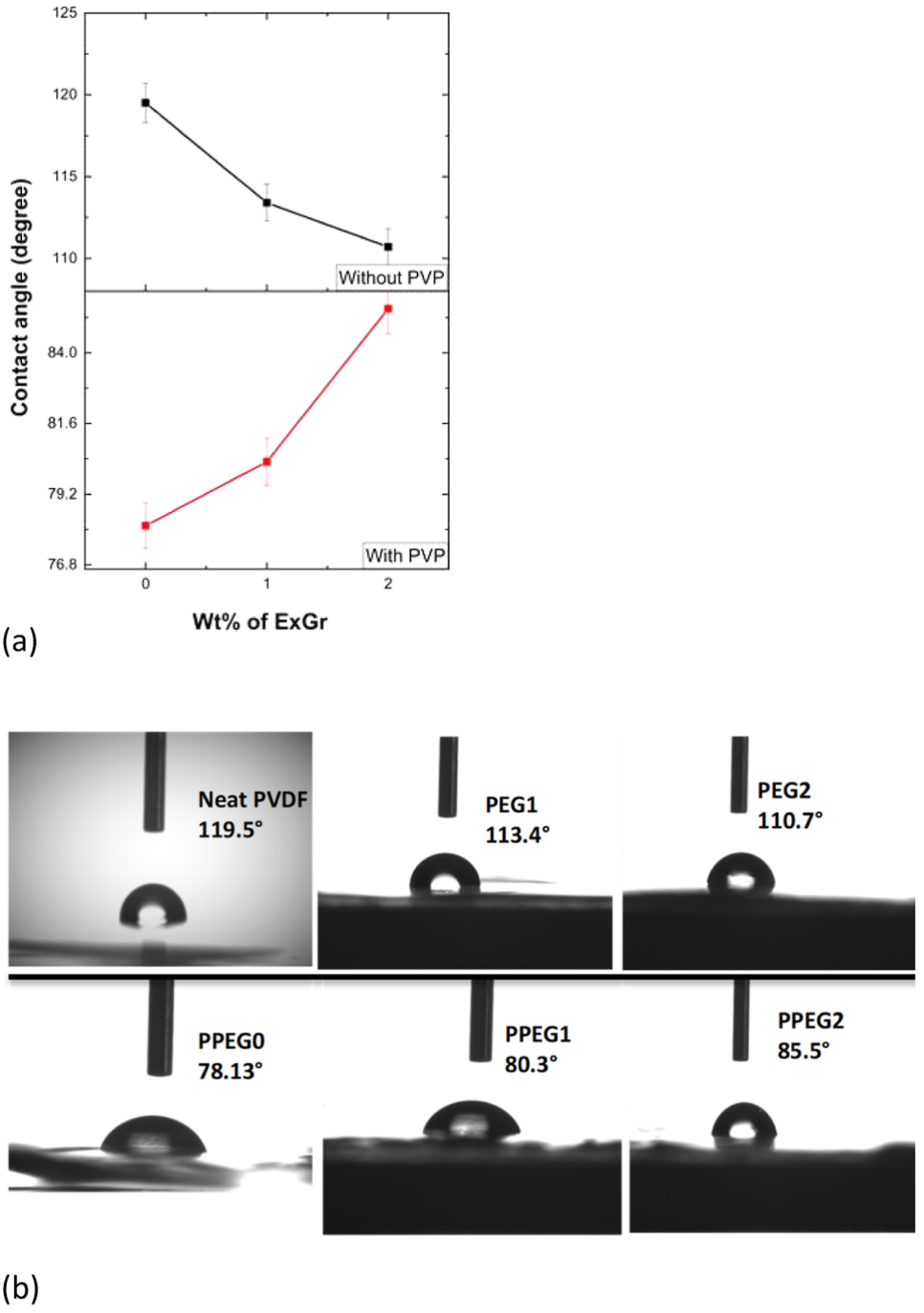

Figure 12. (a) Variation of contact angles with respect to the loadings of ExGr in PVDF-*x* wt % ExGr (*x* = 0, 1, 2) with and without 1 wt % PVP of compression-molded samples. (b) Digital pictures depicting contact angles of compression-molded samples (from top left) neat PVDF, PEG1, PEG2, PPEG0, PPEG1, and PPEG2 composite films.

increased for compression-molded neat PVDF with 1 wt % PVP (86.8%) when compared to that of the same sample without PVP (85.8%). This result suggests the fact that though melt viscosity is decreased, the interaction between PVDF and PVP is appreciable, resulting in higher gamma phase content. A similar trend is observed for compression-molded PEG1 and PPEG1. Since compression molding has been carried out at 240 °C, the coating of PVP chains over GNSs must have been removed, and hence, PVP interacts with PVDF, causing a higher gamma phase content in the composite with PVP (79%). Since the GNSs are distributed randomly, the probability of adhering once again to GNSs would have been reduced. Hence, both PVP chain and GNSs uncoated by PVP can enhance the gamma phase fraction of PVDF. The gamma phase content without PVP in the PVDF-1 wt % ExGr compression-molded sheet is 77.9%. During compression molding, due to a decrease in polymer viscosity, the GNSs can be randomly distributed with an increase in interparticle distance, resulting in decreased electrical conductivity.

Overall, it has been convincingly proved that in compression-molded PVDF-ExGr composites with and without PVP, the electroactive gamma phase content is decreased with an increase in the loading of ExGr. A similar trend has

https://doi.org/10.1021/acsomega.3c03083
ACS Omega 2024, 9, 178−195

been observed for solution-blended samples, also justifying the interaction between PVP and GNSs.

Figure 11d,e depicts a comparison of electroactive phases in PVDF-ExGr composites without and with PVP when two different processing methods are adopted, i.e., solution blending and compression molding. The solution-blending method of the preparation of PVDF-ExGr nanocomposites results in a higher electroactive gamma phase content than compression molding, suggesting that the interaction of solvent molecules with the PVDF chains in the former processing route is significant. Similarly, the electrical conductivities of solution-blended composites are higher than that of compression-molded samples for the same loading of fillers in PVDF.

3.9.4. Contact Angle Analysis of Compression-Molded PVDF-ExGr Nanocomposites. Figure 12a depicts the variation of contact angles of the compression-molded PVDF-ExGr nanocomposite samples. The contact angle of the compression-molded neat PVDF film is 118.9°, which is greater than that of the solvent-cast sample. Upon incorporation of 1 and 2 wt % ExGr in PVDF without PVP followed by compression molding, the contact angle is decreased. Since the compression molding has been carried out at a temperature of 240 °C, the melt viscosity of the polymer will decrease, eventually increasing the interparticular distance of the graphite particles. This results in the decreasing trend of the contact angle in the composite system without PVP. In the case of the composite system with PVP, the contact angle of PPEG0 is 78.13°, supporting the hydrophilic character of the film. This can be due to the presence of PVP on the surface of PVDF sheets as reported elsewhere.[64] Upon addition of 1 and 2 wt % ExGr in PVDF with 1 wt % PVP, the contact angle increases to 80.3 and 85.5°, respectively. Since the dispersion of GNSs is better with the incorporation of PVP, the contact angle increases owing to the increase in surface roughness. Thus, in the presence of PVP, the contact angle shows an increasing trend due to enhanced dispersion of GNSs, whereas the contact angle of compression-molded PVDF-ExGr composites shows a decreasing trend. Thus, the role played by PVP in the dispersion of GNSs in the PVDF matrix is justified. Also, it should be noted that the contact angle of the compression-molded neat PVDF sheet is above 118°, which is due to the coexistence of electroactive gamma and alpha phases, as proved by XRD and FTIR analyses which might result in increased surface roughness. The contact angle of neat PVDF with a nonpolar alpha phase has been reported to be around 90°.[58] The digital pictures of the water droplet on compression-molded PVDF-ExGr with and without PVP are shown in Figure 12b.

It should be mentioned that the WCA of the solvent-cast neat PVDF film is lesser than that of the compression-molded PVDF sheet. The higher WCA for the compression molded sample can be attributed to the fact that a dense packed structure is formed after cooling the melt. In the case of the solvent-cast neat PVDF film, while solvent evaporation, the polymer chain could have been pushed at different regions, causing loosely packed polymer chains, and hence, the contact angle under the identical measuring method has yielded decreased values. In short, it is clear from the above analysis that the WCA of PVDF-ExGr nanocomposites depends on the processing method adopted.

4. CONCLUSIONS

The dispersion of GNSs in PVDF has been enhanced by employing PVP as the surfactant in comparison to the nanocomposites without PVP. The electrical percolation threshold of PVDF-ExGr-1 wt % PVP nanocomposites has been reduced to 0.3 wt % ExGr when compared to that of solution-blended PVDF-ExGr composites (0.5 wt % ExGr.) This result proves that the layer of the surfactant coated over the GNSs is less and that the interparticular distance for the charge transport would have been reduced to a greater extent. The formation of GNSs and enhanced dispersion of GNSs in PVDF due to the incorporation of PVP have been confirmed through FESEM analysis. The existence of the electroactive gamma phase of PVDF in solvent-cast PVDF-ExGr and PVDF-ExGr-1 wt % PVP composites has been confirmed through XRD and FTIR analyses. Both the alpha and gamma phases coexist in PVDF-ExGr nanocomposites. DSC analysis proves the existence of the gamma phase of PVDF as a high-temperature melting peak around 172 °C is observed apart from that of the alpha phase for the investigated PVDF-ExGr nanocomposites. TGA proves the fact that the thermal stability of the composite with PVP is higher than that of composites without PVP above 500 °C as the char content was observed to be higher in the former composites. This is attributed to enhancement in the dispersion of GNSs in the PVDF matrix. Enhanced hydrophobicity of the solvent-cast PVDF-ExGr composites with and without PVP was confirmed by WCA analysis. The electrical conductivity of compression-molded PVDF-ExGr nanocomposites with and without PVP has been observed to be less than that of solution-blended nanocomposites of the same loading of filler particles. The decrease in the melt viscosity of the polymer during compression molding increases the interparticular distance of GNSs, which increases the barrier for the charge transport. The electroactive gamma phase content and the electrical conductivity values of PVDF-expanded graphite nanocomposites suggest the fact that they can be used for mechanical energy harvesting and electromagnetic shielding application in the microwave frequency range.

■ ASSOCIATED CONTENT

Supporting Information

The Supporting Information is available free of charge at https://pubs.acs.org/doi/10.1021/acsomega.3c03083.

Experimental data which includes preparation and characterization techniques utilized for the analysis of PVDF-ExGr nanocomposites with and without PVP (PDF)

■ AUTHOR INFORMATION

Corresponding Author

Ramanujam Brahmadesam Thoopul Srinivasa Raghava − *Department of Sciences, Amrita School of Physical Sciences, Amrita Vishwa Vidyapeetham, Coimbatore 641112, India; Functional Materials Laboratory, Amrita School of Engineering, Amrita Vishwa Vidyapeetham, Coimbatore 641112, India;* orcid.org/0000-0003-0593-0285; Email: bts_ramanujam@cb.amrita.edu

https://doi.org/10.1021/acsomega.3c03083
ACS Omega 2024, 9, 178−195

Authors

Reshma Haridass − *Department of Sciences, Amrita School of Physical Sciences, Amrita Vishwa Vidyapeetham, Coimbatore 641112, India*

Aleena Sabu − *Department of Sciences, Amrita School of Physical Sciences, Amrita Vishwa Vidyapeetham, Coimbatore 641112, India*

Nikhitha Augustin − *Department of Sciences, Amrita School of Physical Sciences, Amrita Vishwa Vidyapeetham, Coimbatore 641112, India*

Pratheep Kumar Annamalai − *School of Agriculture and Environmental Science, University of Southern Queensland, Toowoomba 4350 QLD, Australia; Centre for Future Materials, University of Southern Queensland, Toowoomba, Queensland 4350, Australia;* orcid.org/0000-0002-7284-0813

Complete contact information is available at: https://pubs.acs.org/10.1021/acsomega.3c03083

Funding

This research work did not receive any grant from any funding agencies. One of the Authors R.H. thanks Amrita Vishwa Vidyapeetham for providing consumables such as chemicals for carrying out this work.

Notes

The authors declare no competing financial interest.

■ ACKNOWLEDGMENTS

The authors are grateful to Dr. M. Sivakumar, Department of Sciences, Amrita School of Physical Sciences, Coimbatore, Amrita Vishwa Vidyapeetham for extending his lab facilities which were important for the completion of this work. The authors also extend their gratitude to Senthil Kumar, COE AMGT, Amrita Vishwa Vidyapeetham, Coimbatore for capturing the FESEM pictures of samples examined in this work.

■ REFERENCES

(1) Haridas Menon, N.; Sabu, A.; B, T. S. R. Polyvinylidene fluoride-poly(vinyl acetate)-natural graphite blend nanocomposites: Investigations of electroactive phase formation, electrical, thermal, and wetting properties. *Polym. Adv. Technol.* **2022**, *33* (12), 4023−4040.

(2) Khalifa, M.; Schoeffmann, E.; Lammer, H.; Mahendran, A. R.; Wuzella, G.; Anandhan, S. A study on electroactive PVDF/mica nanosheet composites with an enhanced γ-phase for capacitive and piezoelectric force sensing. *Soft Matter* **2021**, *17*, 10891−10902.

(3) Qi, Q.; Ma, L.; Zhao, B.; Wang, S.; Liu, X.; Lei, Y.; Park, C. B. An Effective Design Strategy for the Sandwich Structure of PVDF/GNP-Ni-CNT Composites with Remarkable Electromagnetic Interference Shielding Effectiveness. *ACS Appl. Mater. Interfaces* **2020**, *12* (32), 36568−36577.

(4) Mohd Radzuan, N. A.; Yusuf Zakaria, M.; Sulong, A. B.; Sahari, J. The effect of milled carbon fibre filler on electrical conductivity in highly conductive polymer composites. *Composites, Part B* **2017**, *110*, 153−160.

(5) Liu, X.; Liu, J.; Lin, B.; Chu, F.; Ren, Y. PVDF-HFP-Based Composite Electrolyte Membranes having High Conductivity and Lithium-Ion Transference Number for Lithium Metal Batteries. *ACS Appl. Energy Mater.* **2022**, *5* (1), 1031−1040.

(6) Strumpler, R.; Glatz-Reichenbach, J. Conducting Polymer Composites. *J. Electroceram.* **1999**, *3* (4), 329−346.

(7) Rasana, N.; Jayanarayanan, K. Polypropylene/short glass fiber/nanosilica hybrid composites: evaluation of morphology, mechanical, thermal, and transport properties. *Polym. Bull.* **2018**, *75*, 2587−2605.

(8) Rasana, N.; Malavika, D.; Aparna, R.; Deepak, T.; Haritha, P. S.; Jayanarayanan, K. Influence of multiphase fillers on mechanical, transport and rheological properties of polypropylene. *Mater. Today: Proc.* **2018**, *5* (8), 16478−16486.

(9) Jayanarayanan, K.; Thomas, S.; Joseph, K. Morphology, static and dynamic mechanical properties of in situ microfibrillar composites based on polypropylene/poly (ethylene terephthalate) blends. *Composites, Part A* **2008**, *39* (2), 164−175.

(10) Li, X.; Wang, X.; Weng, L.; Yu, Y.; Zhang, X.; Liu, L.; Wang, C. Dielectrical properties of graphite nanosheets/PVDF composites regulated by coupling agent. *Mater. Today Commun.* **2019**, *21*, 100705.

(11) Carabineiro, S. A.; Pereira, M. F.; Pereira, J. N.; Caparros, C.; Sencadas, V.; Lanceros Mendez, S. Effect of the carbon nanotube surface characteristics on the conductivity and dielectric constant of carbon nanotube/poly (vinylidene fluoride) composites. *Nanoscale Res. Lett.* **2011**, *6* (1), 302.

(12) Ramanujam, B. T. S.; Adhyapak, P. V.; Radhakrishnan, S.; Marimuthu, R. Effect of casting solvent on the structure development, electrical, thermal behavior of polyvinylidene fluoride (PVDF)−carbon nanofiber (CNF) conducting binary and hybrid nanocomposites. *Polym. Bull.* **2021**, *78*, 1735−1751.

(13) Cho, J.; Lee, H.; Nam, K. H.; Yeo, H.; Yang, C. M.; Seong, D. G.; Lee, D.; Kim, S. Y. Enhanced electrical conductivity of polymer nanocomposite based on edge-selectively functionalized graphene nanoplatelets. *Compos. Sci. Technol.* **2020**, *189*, 108001.

(14) Gong, X.; Liu, J.; Baskaran, S.; Voise, R. D.; Young, J. S. Surfactant-Assisted Processing of Carbon Nanotube/Polymer Composites. *Chem. Mater.* **2000**, *12* (4), 1049−1052.

(15) Lee, S. H.; Cho, E.; Jeon, S. H.; Youn, J. R. Rheological and electrical properties of polypropylene composites containing functionalized multi-walled carbon nanotubes and compatibilizers. *Carbon* **2007**, *45* (14), 2810−2822.

(16) Ma, P. C.; Siddiqui, N. A.; Marom, G.; Kim, J. K. Dispersion and functionalization of carbon nanotubes for polymer-based nanocomposites: A review. *Composites, Part A* **2010**, *41* (10), 1345−1367.

(17) Lovinger, A. J. Ferroelectric Polymers. *Science* **1983**, *220* (4602), 1115−1121.

(18) Abdalla, S.; Obaid, A.; Al-Marzouki, F. M. Preparation and characterization of poly (vinylidene fluoride): A high dielectric performance nanocomposite for electrical storage. *Results Phys.* **2016**, *6*, 617−626.

(19) Li, M.; Wondergem, H. J.; Spijkman, M. J.; Asadi, K.; Katsouras, I.; Blom, P. W. M.; de Leeuw, D. M.; et al. Revisiting the δ-phase of poly (vinylidene fluoride) for solution-processed ferroelectric thin films. *Nat. Mater.* **2013**, *12* (5), 433−438.

(20) Pariy, I. O.; Ivanova, A. A.; Shvartsman, V. V.; Lupascu, D. C.; Sukhorukov, G. B.; Surmeneva, M. A.; Surmenev, R. A. Poling and annealing of piezoelectric Poly (Vinylidene fluoride) micropillar arrays. *Mater. Chem. Phys.* **2020**, *239*, 122035.

(21) Sencadas, V.; Gregorio, R., Jr.; Lanceros-Méndez, S. α to β Phase Transformation and Microestructural Changes of PVDF Films Induced by Uniaxial Stretch. *J. Macromol. Sci., Part B: Phys.* **2009**, *48* (3), 514−525.

(22) Zhang, H.; Zhu, Y.; Li, L. Fabrication of PVDF/graphene composites with enhanced β phase via conventional melt processing assisted by solid state shear milling technology. *RSC Adv.* **2020**, *10* (6), 3391−3401.

(23) Liu, Yi-L.; Li, Y.; Xu, J.-T.; Fan, Z.-Q. Cooperative Effect of Electrospinning and Nanoclay on Formation of polar crystalline phases in poly (vinylidene fluoride). *ACS Appl. Mater. Interfaces* **2010**, *2* (6), 1759−1768.

(24) Liu, X.; Xu, S.; Kuang, X.; Wang, X.-H. Ultra-long MWCNTs highly oriented in electrospun PVDF/MWCNT composite nanofibers with enhanced β phase. *RSC Adv.* **2016**, *6*, 106690−106696.

(25) Cozza, E. S.; Monticelli, O.; Marsano, E.; Cebe, P. On the electrospinning of PVDF: influence of the experimental conditions on the nanofiber properties. *Polym. Int.* **2013**, *62*, 41−48.

(26) Kumar, G. S.; Vishnupriya, D.; Chary, K. S.; Patro, T. U. High dielectric permittivity and improved mechanical and thermal properties of poly(vinylidene fluoride) composites with low carbon nanotube content: effect of composite processing on phase behavior and dielectric properties. *Nanotechnology* **2016**, *27* (38), 385702.
(27) Ramanujam, B. T. S.; Gopalakrishnan, C. Investigations of structure development, electrical and thermal properties of polyvinylidene fluoride-expanded graphite nanocomposites. *Bull. Mater. Sci.* **2021**, *44*, 66.
(28) Sachin, M.; Haridass, R.; Ramanujam, B. T. S. Polyvinylidene fluoride (PVDF)-poly(methyl methacrylate) (PMMA)-expanded graphite (ExGr) conducting polymer blends: Analysis of electrical and thermal behavior. *Mater. Today: Proc.* **2020**, *28* (1), 103−107.
(29) Chung, D. D. L. Review Graphite. *J. Mater. Sci.* **2002**, *37*, 1475−1489.
(30) Biswas, P.; Hoque, N. A.; Thakur, P.; Saikh, M. M.; Roy, S.; Khatun, F.; Bagchi, B.; Das, S. Highly Efficient and Durable Piezoelectric Nanogenerator and Photo-Power Cell Based on CTAB-Modified-Montmorillonite Incorporated PVDF Film. *ACS Sustainable Chem. Eng.* **2019**, *7* (5), 4801−4813.
(31) Ding, Y.; Guo, Z.; Dong, X.; You, H.; Mei, J.; Hou, X.; Liang, Z.; Li, Z. Preparation and Characterization of MWCNTs/PVDF Conductive Membrane with Cross-Linked Polymer PVA and Study on Its Anti-Fouling Performance. *Membranes* **2021**, *11* (9), 703.
(32) Wang, L.; Zhang, L.; Tian, M. Improved polyvinylpyrrolidone (PVP)/graphite nanocomposites by solution compounding and spray drying. *Polym. Adv. Technol.* **2012**, *23* (3), 652−659.
(33) Bentini, R.; Pola, A.; Rizzi, L. G.; Athanassiou, A.; Fragouli, D. A Highly Porous Solvent Free PVDF/Expanded Graphite Foam for Oil/Water Separation. *Chem. Eng. J.* **2019**, *372*, 1174−1182.
(34) Xie, P.; Li, Y.; Qiu, J. Preparation and dielectric behavior of polyvinylidene fluoride composite filled with modified graphite nanoplatelet. *J. Appl. Polym. Sci.* **2014**, *131* (24), 40229.
(35) Zhang, Y.; Rhee, K. Y.; Park, S. J. Facile design of a domestic thermoelectric generator by tailoring the thermoelectric performance of volume-controlled expanded graphite/PVDF composites. *Composites, Part B* **2019**, *176*, 107234.
(36) Li, X.; Wang, X.; Weng, L.; Yu, Y.; Zhang, X.; Liu, L.; Wang, C. Dielectrical properties of graphite nanosheets/PVDF composites regulated by coupling agent. *Mater. Today Commun.* **2019**, *21*, 100705.
(37) Deng, S.; Zhu, Y.; Qi, X.; Yu, W.; Chen, F.; Fu, Q. Preparation of polyvinylidene fluoride/expanded graphite composites with enhanced thermal conductivity via ball milling treatment. *RSC Adv.* **2016**, *6* (51), 45578−45584.
(38) Kou, Y.; Zhou, W.; Li, X.; Wang, Z.; Li, Y.; Cai, H.; Liu, D.; Chen, F.; Wang, G.; Dang, Z. M. Enhanced dielectric properties of PVDF nanocomposites with modified sandwich-like GO@PVP hybrids. *Polym.-Plast. Technol. Mater.* **2020**, *59* (6), 592−605.
(39) El Achaby, M.; Arrakhiz, F. E.; Vaudreuil, S.; Essassi, E. M.; Qaiss, A.; Bousmina, M. Nanocomposite films of poly (vinylidene fluoride) filled with polyvinylpyrrolidone-coated multiwalled carbon nanotubes: Enhancement of β-polymorph formation and tensile properties. *Polym. Eng. Sci.* **2013**, *53* (1), 34−43.
(40) Cai, X.; Lei, T.; Sun, D.; Lin, L. A critical analysis of the α, β and γ phases in poly(vinylidene fluoride) using FTIR. *RSC Adv.* **2017**, *7* (25), 15382−15389.
(41) Martins, P.; Lopes, A. C.; Lanceros-Mendez, S. Electroactive phases of poly (vinylidene fluoride): Determination, processing and applications. *Prog. Polym. Sci.* **2014**, *39* (4), 683−706.
(42) Liu, J.; Lu, X.; Wu, C. Effect of Preparation Methods on Crystallization Behavior and Tensile Strength of Poly(vinylidene fluoride) Membranes. *Membranes* **2013**, *3* (4), 389−405.
(43) Chen, S.; Cheng, B.; Ding, C. Synthesis and Characterization of Poly(vinyl pyrrolidone)/Reduced Graphene Oxide Nanocomposite. *J. Macromol. Sci., Part B: Phys.* **2015**, *54* (4), 481−491.
(44) Zhang, X.; Wang, J.; Jia, H.; Yin, B.; Ding, L.; Xu, Z.; Ji, Q. Polyvinyl pyrrolidone modified graphene oxide for improving the mechanical, thermal conductivity, and solvent resistance properties of natural rubber. *RSC Adv.* **2016**, *6* (60), 54668−54678.
(45) Wajid, A. S.; Das, S.; Irin, F.; Ahmed, H. T.; Shelburne, J. L.; Parviz, D.; Fullerton, R. J.; Jankowski, A. F.; Hedden, R. C.; Green, M. J. Polymer-stabilized graphene dispersions at high concentrations in organic solvents for composite production. *Carbon* **2012**, *50* (2), 526−534.
(46) Yoon, S.; In, I. Role of poly(N-vinyl-2-pyrrolidone) as stabilizer for dispersion of graphene via hydrophobic interaction. *J. Mater. Sci.* **2011**, *46*, 1316−1321.
(47) Guo, Z.; Xu, X.; Xiang, Y.; Lu, S.; Jiang, S. P. New anhydrous proton exchange membranes for high-temperature fuel cells based on PVDF-PVP blended polymers. *J. Mater. Chem. A* **2015**, *3* (1), 148−155.
(48) Kar, E.; Bose, N.; Dutta, B.; Mukherjee, N.; Mukherjee, S. Poly (vinylidene fluoride)/submicron graphite platelet composite: A smart, lightweight flexible material with significantly enhanced β polymorphism, dielectric and microwave shielding properties. *Eur. Polym. J.* **2017**, *90*, 442−455.
(49) Bormashenko, Y.; Pogreb, R.; Stanevsky, O.; Bormashenko, E. Vibrational spectrum of PVDF and its interpretation. *Polym. Test.* **2004**, *23* (7), 791−796.
(50) Ayyappan, J.; Menon, N. H.; Sabu, A.; Ramanujam, B. T. S. Polyvinylidene fluoride-natural graphite flexible composite films: Formation of graphite nanosheets, electroactive phase, analysis of electrical and thermal properties. *Polym. Adv. Technol.* **2022**, *33*, 3997−4011.
(51) Chen, N.; Hong, L. Surface phase morphology and composition of the casting films of PVDF-PVP blend. *Polymer* **2002**, *43* (4), 1429−1436.
(52) Mondal, D.; Mollick, M. M. R.; Bhowmick, B.; Maity, D.; Bain, M. K.; Rana, D.; Mukhopadhyay, A.; Dana, K.; Chattopadhyay, D. Effect of poly(vinylpyrrolidone) on the morphology and physical properties of poly(vinylalcohol)/sodium montmorillonite nanocomposite films. *Prog. Nat. Sci.* **2013**, *23* (6), 579−587.
(53) Alibe, I. M.; Matori, K. A.; Sidek, H. A. A.; Yaakob, Y.; Rashid, U.; Alibe, A. M.; Zaid, M. H. M.; Nasir, S.; Nasir, M. M. Effects of polyvinylpyrrolidone on structural and optical properties of willemite semiconductor nanoparticles by polymer thermal treatment method. *J. Therm. Anal.* **2019**, *136*, 2249−2268.
(54) Loría-Bastarrachea, M. I.; Herrera-Kao, W.; Cauich-Rodríguez, J. V.; et al. A TG/FTIR study on the thermal degradation of poly (vinyl pyrrolidone). *J. Therm. Anal. Calorim.* **2016**, *104* (2), 737−742.
(55) Li, W.; Li, H.; Zhang, Y. M. Preparation and investigation of PVDF/PMMA/TiO2 composite film. *J. Mater. Sci.* **2009**, *44* (11), 2977−2984.
(56) Nguyen, T. Degradation of poly[vinyl fluoride] and poly-[vinylidene fluoride]. *J. Macromol. Sci., Chem.* **1985**, *25*, 227−275.
(57) De Jesus Silva, A. J.; Contreras, M. M.; Nascimento, C. R.; Da Costa, M. F. Kinetics of thermal degradation and lifetime study of poly (vinylidene fluoride) (PVDF) subjected to bioethanol fuel accelerated aging. *Heliyon* **2020**, *6* (7), No. e04573.
(58) Kumar, A. P.; Depan, D.; Singh Tomer, N.; Singh, R. P. Nanoscale particles for polymer degradation and stabilization—Trends and future perspectives. *Prog. Polym. Sci.* **2009**, *34* (6), 479−515.
(59) Chakradhar, R. P. S.; Prasad, G.; Bera, P.; Anandan, C. Stable superhydrophobic coatings using PVDF-MWCNT nanocomposite. *Appl. Surf. Sci.* **2014**, *301*, 208−215.
(60) Gupta, D.; Gulrajani, M. L. Self-cleaning finishes for textiles. *Functional Finishes for Textiles*, 1st ed.; Paul, R., Ed.; Woodhead Publishing: Cambridge, 2015; pp 257−281.
(61) Huang, Z. X.; Liu, X.; Wong, S. C.; Qu, J. Electrospinning polyvinylidene fluoride/expanded graphite composite membranes as high efficiency and reusable water harvester. *Mater. Lett.* **2017**, *202*, 78−81.
(62) Zhao, X.; Cheng, J.; Chen, S.; Zhang, J.; Wang, X. Hydrophilic modification of poly(vinylidene fluoride) (PVDF) by in situ

https://doi.org/10.1021/acsomega.3c03083
ACS Omega 2024, 9, 178−195

polymerization of methyl methacrylate (MMA) monomer. *Colloid Polym. Sci.* **2010**, *288* (12−13), 1327−1332.
(63) Silva, M. P.; Sencadas, V.; Botelho, G.; Machado, A. V.; Rolo, A. G.; Rocha, J. G.; Lanceros-Mendez, S. α- and γ-PVDF: Crystallization kinetics, microstructural variations and thermal behaviour. *Mater. Chem. Phys.* **2010**, *122* (1), 87−92.
(64) Peng, Q.; Tan, X.; Venkataraman, M.; Militky, J. Tailored expanded graphite based PVDF porous composites for potential electrostatic dissipation applications. *Diamond Relat. Mater.* **2022**, *125*, 108972.

https://doi.org/10.1021/acsomega.3c03083
ACS Omega 2024, 9, 178−195